# Reciprocal discoidin domain receptor signaling strengthens integrin adhesion to connect adjacent tissues

[#]Kieop Park[1], [#]Ranjay Jayadev[1], [#]Sara G. Payne[1,2], Isabel W. Kenny-Ganzert[1], Qiuyi Chi[1], Daniel S. Costa[1], William Ramos-Lewis[1], Siddharthan Balachandar Thendral[1], and [*]David R. Sherwood[1]

[1] Department of Biology, Duke University, Box 90338, Durham, NC 27708, USA

[2] Department of Cell Biology, Duke University Medical Center, Durham, NC 27708, USA

[#]Shared first author
[*]Correspondence: david.sherwood@duke.edu

Running title: DDR-2 signaling connects tissues

Key words: Discoidin domain receptor, type IV collagen, integrin, endocytosis, Ras, basement membrane, tissue connection

## Abstract

Separate tissues connect through adjoining basement membranes to carry out molecular barrier, exchange, and organ support functions. Cell adhesion at these connections must be robust and balanced to withstand independent tissue movement. Yet, how cells achieve synchronized adhesion to connect tissues is unknown. Here, we have investigated this question using the *C. elegans* utse-seam tissue connection that supports the uterus during egg-laying. Through genetics, quantitative fluorescence, and cell specific molecular disruption, we show that type IV collagen, which fastens the linkage, also activates the collagen receptor discoidin domain receptor 2 (DDR-2) in both the utse and seam. RNAi depletion, genome editing, and photobleaching experiments revealed that DDR-2 signals through LET-60/Ras to coordinately strengthen an integrin adhesion in the utse and seam that stabilizes their connection. These results uncover a synchronizing mechanism for robust adhesion during tissue connection, where collagen both affixes the linkage and signals to both tissues to bolster their adhesion.

52 **Introduction**

53 Basement membrane (BM) is a planar, cell-associated extracellular matrix (ECM) that underlies
54 or surrounds most tissues. BM provides tissues with structural support, barrier functions, and
55 signaling platforms (Morrissey and Sherwood 2015, Jayadev and Sherwood 2017, Pozzi,
56 Yurchenco et al. 2017). The two core BM matrix components are the heterotrimeric proteins
57 laminin and type IV collagen. Laminin is comprised of an α, β, and γ subunit. Once secreted,
58 laminin associates with cell surface receptors and self-assembles into a sheet-like network.
59 Type IV collagen is a large protein comprised of two α1-like and one α2-like chains, and these
60 heterotrimers cross-link to form a grid, which is thought to be connected to the laminin network
61 through bridging molecules (Hohenester and Yurchenco 2013). Type IV collagen provides BM
62 with tensile strength, which allows BM to structurally support tissues and resist mechanical
63 forces (Fidler, Boudko et al. 2018). Type IV collagen is a ligand for several vertebrate integrin
64 receptors and the collagen-specific receptor tyrosine kinase discoidin domain receptor 1 (DDR1)
65 (Khoshnoodi, Pedchenko et al. 2008, Brown, Cummings et al. 2017). Integrin and DDR1
66 interactions with type IV collagen mediate a wide variety cell-matrix functions, including cell
67 migration and cell adhesion (Khoshnoodi, Pedchenko et al. 2008, Castro-Sanchez, Soto-
68 Guzman et al. 2010, Borza and Pozzi 2014, Xiao, Jiang et al. 2015). DDR receptors and integrin
69 also functionally interact within cells (Leitinger 2014); however, the roles of these interactions in
70 native tissue settings remains poorly defined.

71

72 At tissue interfaces juxtaposed BMs usually slide along each other and maintain distinct tissue
73 boundaries (Sherwood and Sternberg 2003, Brown 2011). At specific sites, however, the BMs of
74 neighboring tissues link to stabilize tissue interactions and build complex organs (Keeley and
75 Sherwood 2019). Examples include the kidney, where podocytes and endothelial BMs connect
76 to form the glomerular BM blood filtration unit (Abrahamson 1985); the brain, where the
77 astrocyte end feet and endothelial BMs join to build the blood-brain barrier (Sixt, Engelhardt et

al. 2001); and the somite, where somite and epidermal BMs link to maintain somite-epidermal association during development (Feitosa, Zhang et al. 2012). Approximately 20 different BM-BM linkages between neighboring tissues have been documented (Gao, Mruk et al. 2017, Keeley and Sherwood 2019, Welcker, Stein et al. 2021). Disruption of these BM-BM tissue connections appear to underlie human diseases, such as in Alport's syndrome, where defects in kidney and hearing are associated with tissue linkage disruption (Merchant, Burgess et al. 2004, Naylor, Morais et al. 2021). Despite the prevalence and importance of BM-BM tissue connections, the challenge of studying tissue interactions *in vivo* in vivo has hampered our understanding of the mechanisms establishing and maintaining these linkages.

The simple tissues, visual transparency, and experimental tractability of *C. elegans* offers a powerful model to study BM-BM tissue interactions. Further, most *C. elegans* BM components and receptors are endogenously tagged with genetically encoded fluorophores to visualize localization, levels, and dynamics (Keeley, Hastie et al. 2020, Jayadev, Morais et al. 2022). A stable BM-BM tissue connection between the large, multinucleated uterine utse cell and epidermal seam cells stabilizes the uterus during egg laying (Vogel and Hedgecock 2001, Morrissey, Keeley et al. 2014, Gianakas, Keeley et al. 2023). Disruption of the utse-seam BM-BM tissue linkage results in prolapse of the uterus (**Rup**tured phenotype) out of the animal during egg-laying. Formation of the utse-seam attachment is initiated by the deposition of the matrix proteins fibulin and hemicentin during the last larval stage of development. Hemicentin promotes the recruitment of type IV collagen, which accumulates at high levels at the BM-BM tissue connection and strengthens the adhesion, allowing it to resist the strong mechanical forces of egg-laying (Gianakas, Keeley et al. 2023). The integrin, αINA-1, one of two *C. elegans* alpha integrins, is also expressed in the utse and is required to prevent uterine-prolapse during egg-laying. However, its regulation and function at the utse-seam connection is unclear (Morrissey, Keeley et al. 2014, Gianakas, Keeley et al. 2023). Mechanisms that link juxtaposed

104 BMs appear to be shared, as hemicentin-1 promotes BM-BM tissue connection in the zebrafish
105 fin fold, hemicentin-2 and fibulin-1 mediate zebrafish somite-epidermis BM-BM association, and
106 hemicentin-1 stabilizes BM-BM linkage at myotendinous junctions in mice (Carney, Feitosa et
107 al. 2010, Feitosa, Zhang et al. 2012, Welcker, Stein et al. 2021). In addition, type IV collagen
108 bridges the podocyte BM and endothelial BM to form the glomerular BM in mice and humans
109 (Suleiman, Zhang et al. 2013, Naylor, Morais et al. 2021). While significant insights are being
110 gained on matrix composition at BM-BM tissue connections, it remains unknown how tissues
111 coordinate and strengthen their adhesive activity at linkage sites. Cells at tissue connections
112 must resist the forces of tissue shifting arising from growth, muscle contraction, and blood flow,
113 and it is unclear how tissues synchronize and bolster adhesions at tissue linkage sites.
114
115 Here, we discover that the *C. elegans* discoidin domain receptor DDR-2, an ortholog to the two
116 vertebrate collagen binding DDR tyrosine kinase receptors (RTK), coordinates and strengthens
117 an integrin mediated cell adhesion to support the utse-seam BM-BM tissue linkage during its
118 formation. Using genetics, endogenous tagging, and tissue-specific molecular perturbations, we
119 show that DDR-2 is expressed and functions in the utse and seam cells to mediate utse-seam
120 attachment between the mid and late L4 larval stages. We reveal that assembly of type IV
121 collagen linking the juxtaposed BMs triggers the internalization of DDR-2 in both the utse and
122 seam cells into endocytic vesicles, a signaling compartment for DDR/RTK receptors. In the *ddr-*
123 *2* knockout mutant, gaps in utse-seam attachment occurred at this time. Through tissue-specific
124 perturbation, quantitative fluorescence analysis, and fluorescence recovery after photobleaching
125 (FRAP), we provide evidence that DDR-2 signals through LET-60/Ras to increase the levels
126 and stability of the α-integrin INA-1 at the utse-seam linkage. Together, these results reveal a
127 mechanism for synchronizing a robust adhesion during tissue linkage, where type IV collagen,
128 which bridges and fastens the BM-BM tissue linkage, also serves as a signal to coordinate and
129 bolster cell-matrix adhesion in cells on both sides of the tissue connection.

130 ## Results

131 **The utse and seam cells associate during the early-L4 stage**

132 The utse is an H-shaped syncytial uterine cell that underlies the *C. elegans* uterus and opens
133 along the central crossbar region during egg-laying to allow embryo passage (Ghosh and
134 Sternberg 2014). The utse is flanked laterally on both sides of the animal by a string of
135 epidermal seam cells that run the length of the body. The utse cell and seam cells are each
136 encased in a BM, which become linked by a specialized matrix whose known functional
137 components include hemicentin, fibulin, and type IV collagen (***Figure 1A***) (Gianakas, Keeley et
138 al. 2023). The BM-BM tissue connection supports the uterus during egg-laying and disruption of
139 the linkage results in uterine prolapse (***Figure 1B and C***) (Vogel and Hedgecock 2001). The
140 utse and seam cells are in contact by the mid L4 larval stage (Gianakas, Keeley et al. 2023), but
141 when the initial contact is established is not known.

142

143 The utse is formed from the fusion of one specialized uterine cell, the anchor cell, with eight
144 adjacent uterine pi cell progeny, forming the syncytial nine-nuclei utse during the early L4 stage
145 (Newman, White et al. 1996, Ghosh and Sternberg 2014). To determine when the utse first
146 contacts the seam cells, we used an anchor cell-specific mCherry fluorophore marker (*cdh-*
147 *3p::mCherry::PLC*$\delta^{PH}$; ***Figure 1D***, arrow) (Hagedorn, Yashiro et al. 2009) that diffuses into the
148 uterine pi cell progeny during fusion and simultaneously viewed a GFP seam cell marker
149 (*scmp::GFP::CAAX*) (Chapman, Li et al. 2008). We found that the utse contacts the seam cells
150 during the early L4 stage as the utse syncytium forms (***Figure 1D***, arrowheads; n=5/5 cases
151 observed). Shortly after utse-seam contact, the BM-BM linkage is initiated at the mid L4 stage
152 by the assembly of low levels of hemicentin, which is secreted by the utse and fibulin-1, which
153 hemicentin recruits from the extracellular fluid. Fibulin-1 and hemicentin protect the utse-seam
154 cell connection from mechanical forces arising from body movement and uterine and vulval

155 muscle contractions prior to egg-laying (Gianakas et al. 2023). Hemicentin also promotes
156 recruitment of type IV collagen from the extracellular fluid, which allows the utse-seam BM-BM
157 connection to resist the strong mechanical forces from egg-laying (Gianakas et al. 2023)
158 (***Figure 1D***). Together, these results show that the utse and seam cells are in contact prior to
159 deposition of matrix components that strengthen the utse-seam BM-BM tissue connection.

160

161 **Loss of discoidin domain receptor-2 (DDR-2) causes uterine prolapse**

162 As type IV collagen is critical to the BM-BM connection, we were next interested in
163 understanding how receptors for type IV collagen regulate the utse-seam BM-BM linkage. The
164 two main receptors for type IV collagen are integrin and the discoidin domain receptor (DDR)
165 (Fidler, Boudko et al. 2018). *C. elegans* harbor two integrin heterodimers composed of different
166 α chains with a shared β chain: αINA-1/ βPAT-3 and αPAT-2/ βPAT-3 (Clay and Sherwood
167 2015). The integrin INA-1 is expressed in the utse and its loss leads to uterine prolapse,
168 suggesting a possible role in utse-seam attachment (Morrissey, Keeley et al. 2014, Gianakas,
169 Keeley et al. 2023). Whether DDRs function at the utse-seam connection, however, is unknown.

170

171 *C. elegans* have two DDR genes, *ddr-1* and *ddr-2,* which are paralogs and orthologs to the two
172 mammalian DDRs (Vogel, Abdulhussein et al. 2006). Like mammalian counterparts, the *C.*
173 *elegans* DDRs are comprised of discoidin and discoidin-like domains, followed by a
174 transmembrane domain and a kinase domain (***Figure 2A***). To determine if *C. elegans* DDRs
175 play a role in utse-seam BM-BM linkage, we examined several *ddr-1* and *ddr-2* mutants (***Figure***
176 ***2A***). We first screened for the Rup phenotype caused by uterine prolapse. Animals harboring
177 the *ddr-1(ok874)* deletion allele, which eliminates the intracellular portion of DDR-1, and animals
178 with the *ddr-1(tm382)* allele containing an early stop codon truncating the majority of the
179 predicted protein (Unsoeld, Park et al. 2013), did not show a Rup phenotype (***Figure 2A and***

180 ***B***). In contrast, animals homozygous for the *ddr-2(tm797)* allele, which introduces an early stop
181 codon and is thought to be a null or strong loss-of-function (Unsoeld, Park et al. 2013), exhibited
182 a significant Rup/uterine prolapse defect. Animals carrying the *ddr-2(ok574)* allele, which
183 deletes a portion of the intracellular kinase domain (Unsoeld, Park et al. 2013), also trended
184 towards displaying a significant Rup phenotype (***Figure 2A and B***). We further generated a full-
185 length *ddr-2* deletion allele, *ddr-2(qy64)*, and confirmed that complete loss of *ddr-2* led to
186 penetrant uterine prolapse (***Figure 2A and B***). Taken together, these results indicate that DDR-
187 2 protects against uterine prolapse and may play a role in mediating utse-seam BM-BM
188 attachment.

189

190 **DDR-2 maintains utse-seam attachment during formation of the tissue connection**

191 To determine if the Rup phenotype observed in *ddr-2* mutants is a result of perturbations in the
192 utse-seam BM-BM tissue connection, we examined utse-seam association from the late L3
193 through young adult stages in animals harboring the *ddr-2*(*qy64)* deletion allele (***Figure 2C***). We
194 visualized utse-seam association using the utse and seam cell membrane markers *cdh-*
195 *3p::mCherry::PLC*$\delta^{PH}$ and *scmp::GFP::CAAX,* respectively. Animals homozygous for *ddr-*
196 *2(qy64)* had normal utse-seam cell association at the early L4 stage; however, beginning at the
197 mid L4 stage, gaps in the utse-seam attachment were detected in about 30% of animals. The
198 frequency of gaps increased to ~40% of animals by the mid-to-late L4 and persisted at a similar
199 penetrance to young adulthood (***Figure 2C and D***). These observations suggest that DDR-2
200 functions around the mid L4 to late L4 stages to promote utse-seam attachment. Next, we
201 wanted to determine if the utse-seam detachment observed in *ddr-2(qy64)* mutants led to
202 uterine prolapse. Wild-type and *ddr-2(qy64)* animals were assessed at the L4 larval stage for
203 utse-seam attachment defects and tracked to the 72-hour adult stage, where they were

204 examined for the Rup phenotype. All wild-type L4 larvae had intact utse-seam attachment and
205 did not rupture by 72-hour adulthood (n=8/8 animals). However, among nine *ddr-2(qy64)* mutant
206 animals examined, four exhibited utse-seam detachments at the L4 stage, all of which
207 underwent uterine prolapse (Rup) by adulthood. The remaining five *ddr-2* mutant animals, which
208 had an intact utse-seam linkage, did not display the Rup phenotype. Taken together, these
209 results suggest that DDR-2 promotes utse-seam attachment during early stages of tissue
210 linkage.

211

212 **DDR-2 is found within endocytic vesicles in the utse and seam cells during initial stages**
213 **of tissue attachment**

214 As utse-seam detachment in *ddr-2* mutant animals was first observed at the mid L4 larval stage,
215 we next sought to determine if DDR-2 was expressed in the utse, seam, or both cell types at
216 this time. Between the mid L4 and late L4 stage, the utse-seam tissue connection forms into a
217 tongue-and-groove association between the utse (tongue) and seam (groove) (***Figure 2D and***
218 ***Figure 2—video 1***). To resolve whether DDR2 is localized within the seam, utse, or both (Vogel
219 and Hedgecock 2001), we used either a utse (*cdh-3p::mCherry::PLC*$\delta^{PH}$) or seam cell marker
220 (*scmp::2xmKate2::PLC*$\delta^{PH}$), and imaged endogenously tagged DDR-2 protein (DDR-2::mNG)
221 (Keeley, Hastie et al. 2020) in lateral confocal sections from the L4 to young adult stages
222 (***Figure 3A***). We first examined the seam cells contacting the utse (***Figure 3B***). At the early L4
223 stage DDR-2::mNG was faintly visible at the surface of the seam cells and found in a few
224 intracellular punctae (***Figure 3B*****,** n=10/10 animals). By the mid L4 stage, DDR-2 was
225 predominantly found in punctae in the region of attachment with the utse. Levels of punctae
226 increased until the late L4 stage and then declined sharply by the young adult (***Figure 3B***).
227 Notably, at the late L4, when DDR-2 punctate localization was at its highest, we could not detect
228 any DDR-2 signal at the cell surface (***Figure 3B,*** n = 9/9). We further examined DDR-2::mNG in

229 seam cells that were not contacting the utse and found that DDR-2 levels were uniformly low
230 from the early L4 through the young adult stages (***Figure 3—figure supplement 1A***). We next
231 investigated DDR-2 localization in the utse contacting the seam. Like the seam cells at the
232 tissue connection site, DDR-2 in the utse was punctate and peaked in levels between the mid
233 and late L4 stages and then declined rapidly (***Figure 3C***). We conclude that DDR-2 is present at
234 high levels and localized within punctate structures in the seam and utse cells at the time when
235 utse-seam defects are observed in *ddr-2* mutant animals.
236
237 Receptor tyrosine kinases (RTKs), including DDRs, are activated upon ligand binding and then
238 rapidly internalized into endocytic vesicles: first the early endosome (marked by RAB-5),
239 followed by subsequent sorting for either lysosome-mediated degradation via late endosomes
240 (marked by RAB-7), or recycled back to the cell surface in recycling endosomes (marked by
241 RAB-11) (Goh and Sorkin 2013). In vertebrates, the exposure of cells to collagen results in the
242 internalization of DDR1b into Rab5a positive early endosomes (Mihai, Chotani et al. 2009).
243 Phosphorylation of DDR1 does not occur until the onset of endocytosis and recycling,
244 suggesting that receptor activation occurs in endocytic vesicles (Mihai, Chotani et al. 2009, Fu,
245 Valiathan et al. 2013). As *C. elegans* DDR-2 appeared to be functioning during the mid L4 to
246 late L4 stages, when levels of DDR-2 were highest and present in vesicular structures, we
247 sought to determine whether DDR-2 was internalized within endocytic vesicles. We examined
248 localization of DDR-2::mNG punctae in relation to utse-expressed markers of early endosomes
249 (*cdh-3p::mCherry::rab-5*), late endosomes (*cdh-3p::mCherry::rab-7*), and recycling endosomes
250 (*cdh-3p::mCherry::rab-11*) (Sato, Norris et al. 2014). DDR-2 was co-localized with all three
251 classes of endosomes in the utse, with the highest overlap with RAB-5 early endosomes
252 (***Figure 3—figure supplement 1B***). In addition, we examined an early endosome marker
253 expressed in seam cells (*scmp::mKate2::rab-5*) and observed DDR-2::mNG punctae co-
254 localized with RAB-5 vesicles (***Figure 3—figure supplement 1C***). The presence of DDR-2 in

255 endocytic vesicles within the utse and seam suggested that DDR-2 signaling may be required
256 for utse-seam attachment. Consistent with this, animals harboring the *ddr-2(ok574)* mutant
257 allele, where a portion of the intracellular kinase domain is deleted (***Figure 2A***), exhibited
258 significant utse-seam detachments at the late L4 stage (***Figure 4A***). Taken together, these
259 observations suggest that DDR-2 functions in the utse and seam cells to promote attachment at
260 the tissue linkage site between the mid and late L4 stages, where it may signal within endocytic
261 vesicles.

262

263 **Type IV collagen promotes DDR-2 vesiculation**

264 DDR signaling is triggered by collagen binding, and vertebrate DDRs bind multiple collagens
265 with different binding affinities (Leitinger 2014). Genetic interaction studies in *C. elegans*
266 revealed that transmembrane collagen COL-99, which is most similar to transmembrane
267 collagen type XIII, XXIII, and XXV in vertebrates (Tu, Huhtala et al. 2015), may act as a ligand
268 for *C. elegans* DDR-1 and DDR-2 during axon guidance and that type IV collagen might act as a
269 ligand for DDR-2 during axon regeneration (Hisamoto, Nagamori et al. 2016, Taylor, Unsoeld et
270 al. 2018). *C. elegans* BMs also harbor type XVIII collagen (CLE-1) (Keeley, Hastie et al. 2020).
271 Thus, we next investigated whether any of these cell and BM-associated collagens could
272 function as a ligand for DDR-2 at the utse-seam BM-BM tissue connection site.

273

274 Type IV collagen enriches at the utse-seam BM-BM linkage during its maturation and helps the
275 connected tissues resist the mechanical forces of egg-laying. In contrast, type XVIII collagen is
276 not present enriched at the linkage (Gianakas, Keeley et al. 2023). Whether COL-99 localizes to
277 the utse-seam tissue linkage is unknown. We thus first examined an endogenously tagged
278 COL-99 (mNG::COL-99) (Jayadev, Morais et al. 2022) and compared its localization and levels
279 to type IV collagen ($\alpha$1-type IV collagen::mNG (EMB-9::mNG)) and type XVIII collagen (CLE-

280 1::mNG) (Keeley, Hastie et al. 2020) at the utse-seam connection in late L4 animals. COL-99
281 was not detected while EMB-9 was present at nearly 8-fold higher levels than CLE-1,
282 suggesting that type IV collagen might be the ligand for DDR-2 (***Figure 4B***). Furthermore, the
283 enrichment of type IV collagen levels at the utse-seam connection site occurs rapidly from the
284 mid L4 to late L4 stage (Gianakas, Keeley et al. 2023), correlating with the buildup of DDR-2 in
285 endosomes in the utse and seam cells.
286
287 As exposure to collagen triggers vesiculation of vertebrate DDR1b into endocytic vesicles, we
288 wanted to determine whether type IV collagen controls vesiculation of DDR-2 at the utse-seam
289 BM-BM connection. RNAi-mediated depletion of type IV collagen from the L1 through the late
290 L4 larval stages resulted in a sharp decrease in vesicular DDR-2::mNG in the utse and seam
291 cells at the linkage site, accompanied by enrichment of DDR-2 at cell surfaces (***Figure 4C;***
292 ***Figure 4—figure supplement 1A***). In contrast, reduction of COL-99 and type XVIII collagen did
293 not significantly affect DDR-2 vesiculation (***Figure 4C; Figure 4—figure supplement 1B and***
294 ***C***). Depletion of hemicentin, which plays a crucial role in recruiting type IV collagen to the BM-
295 BM linking matrix (Gianakas, Keeley et al. 2023), also resulted in a significant reduction in DDR-
296 2 vesiculation (***Figure 4D; Figure 4—figure supplement 1D***). In addition, we did not detect
297 DDR-2 at the cell surface, suggesting that hemicentin has a role in recruiting DDR-2 to the site
298 of utse-seam attachment. Together, these findings indicate that type IV collagen assembly at
299 the site of utse-seam BM-BM tissue linkage triggers DDR-2 vesiculation and may act as a ligand
300 for DDR-2 activation to promote utse-seam attachment.
301
302 **DDR-2 functions in the utse and the seam to promote utse-seam attachment**
303 Since DDR-2 localizes to both the utse and seam cells, we next investigated where DDR-2
304 functions to promote utse-seam BM-BM attachment. We generated genome edited lines with
305 single-copy insertions of dominant negative (DN) *ddr-2* (Bernadskaya, Brahmbhatt et al. 2019)

306 driven by the *cdh-3* promoter for utse expression or the *scm* promoter for seam expression.
307 Using the utse-specific membrane marker (*nas-22p::2xmKate2::PLC*$\delta^{PH}$) (Park, Pan et al. 2010)
308 and a seam cell membrane marker (*wrt-2p::GFP::PLC*$\delta^{PH}$) (Wildwater, Sander et al. 2011), we
309 found significant utse-seam detachments in both utse-expressed and seam-expressed *DN ddr-2*
310 animals at the late L4 stage (***Figure 4F and G***). Consistent with the timing and vesicular pattern
311 of DDR-2 localization, these results indicate that DDR-2 functions in both the utse and seam
312 between the mid and late L4 stages to promote utse-seam attachment.

313

314 **Loss of DDR-2 increases type IV collagen at the utse-seam BM-BM adhesion site**

315 The matrix components fibulin-1 and hemicentin play early roles in mediating utse-seam
316 attachment and hemicentin promotes recruitment of type IV collagen and further enrichment of
317 fibulin, which strengthens the BM-BM attachment (Gianakas et al. 2023). We thus next asked
318 whether DDR-2 promotes utse-seam linkage by regulating the assembly of fibulin, hemicentin,
319 or type IV collagen at the connecting matrix. Knockdown of *ddr-2* by RNAi did not alter fibulin
320 levels at the late L4 stage (***Figure 5—figure supplement 1A and B***). However, we observed a
321 modest ~20% reduction in hemicentin upon depletion of DDR-2 (***Figure 5—figure supplement***
322 ***1C***). As loss of hemicentin results in utse-seam detachment at the late L4 stage (Gianakas,
323 Keeley et al. 2023), we tested whether a ~20% reduction of hemicentin could cause these
324 defects by initiating RNAi at the early L4, just before the utse forms (***Methods***). We found that
325 utse-seam attachments were intact in all animals at the late L4 stage upon ~20% reduction of
326 hemicentin (n=13/13 and 12/12 control and *him-4* RNAi-treated animals examined respectively;
327 ***Figure 5—figure supplement 1D***), suggesting that the utse-seam detachment defect in *ddr-2*
328 mutant animals is not caused by a modest reduction in hemicentin levels. Interestingly, there
329 was an ~40% increase in type IV collagen levels at the utse-seam connection after RNAi
330 mediated reduction of *ddr-2*, indicating a possible feedback mechanism between DDR-2

331 signaling and collagen assembly (***Figure 5—figure supplement 1E***). In sum, these results
332 indicate that knockdown of *ddr-2* does not decrease the functional levels of key matrix
333 components at the site of utse-seam BM-BM connection, suggesting that DDR-2 does not
334 promote utse-seam attachment by regulating the assembly of the BM-BM linking matrix.

335

336 **DDR-2 promotes integrin function to mediate utse-seam tissue attachment**

337 Studies have indicated that vertebrate DDRs are not strong adhesive receptors (Xu, Bihan et al.
338 2012). Consistent with this, we detected weak DDR-2::mNG fluorescence signals at the cell
339 membranes of the utse and seam. However, we observed strong DDR-2 signals in a vesicular
340 pattern in both tissues. We thus assessed several molecular activities regulated by DDR
341 signaling that might mediate utse-seam attachment. Vertebrate DDRs promote matrix
342 metalloproteinase (MMP) expression and localization (Leitinger 2014). The *C. elegans* genome
343 harbors six MMP genes, named zinc metalloproteinase 1-6 (*zmp-1-6*) (Altincicek, Fischer et al.
344 2010). We examined four available reporters of ZMP localization (ZMP-1::GFP, ZMP-2::GFP,
345 ZMP-3::GFP, and ZMP-4::GFP) (Kelley, Chi et al. 2019). Only ZMP-4 was detected at the utse-
346 seam connection and its localization was not altered by knockdown of *ddr-2* (***Figure 5—figure***
347 ***supplement 1F***), suggesting that DDR-2 does not promote utse-seam linkage through
348 regulation of MMPs.

349

350 DDRs also modulate integrin activity (Leitinger 2014). Cell culture studies have shown that
351 vertebrate DDRs can enhance integrin adhesion and integrin cell surface levels in multiple cell
352 types (Xu, Bihan et al. 2012, Staudinger, Spano et al. 2013, Bayer, Grither et al. 2019). *C.*
353 *elegans* harbor only two integrin receptors, made up of either the α subunit INA-1 or PAT-2
354 dimerized to the sole β subunit PAT-3 (Clay and Sherwood 2015). We previously found that
355 depletion of INA-1 results in a Rup phenotype, but the specific effect on utse-seam BM-BM

356 tissue attachment was not determined (Morrissey, Keeley et al. 2014). Thus, we next asked
357 whether DDR-2 promotes utse-seam attachment through regulation of integrin. First, we
358 analyzed the localization and levels of endogenously tagged INA-1 (αINA-1::mNG) and PAT-2
359 (αPAT-2::2xmNG) (Jayadev, Chi et al. 2019) and found that both integrin α subunits were
360 expressed in the utse and seam tissues and localized to the utse-seam connection region from
361 the mid-L4 stage through young adulthood (***Figure 5A and B; Figure 5—figure supplement***
362 ***2A and B***). Their levels mirrored that of DDR-2, with a peak at the late L4 stage, followed by a
363 drop off in the young adult stage (***Figure 5A and B)***. However, INA-1 levels were at least sixfold
364 greater than PAT-2 (note, each PAT-2 is linked to two mNG molecules, see ***Methods***),
365 suggesting it may have a dominant role in adhesion (***Figure 5A and B***). Loss of *ddr-2* resulted
366 in a significant reduction in levels of both INA-1 and PAT-2 at the utse-seam BM-BM attachment
367 through the L4 larval stage (***Figure 5B***). Taken together these data suggest DDR-2 could
368 function to promote integrin adhesion within each tissue at the utse-seam connection.
369
370 We focused on a possible role for DDR-2 in regulating INA-1 at the utse-seam linkage, as INA-1
371 was present at higher levels compared to PAT-2 (***Figure 5A and B***) and was more enriched at
372 cell surfaces (***Figure 5—figure supplement 2C***). Furthermore, PAT-2 anchors muscle
373 attachments (Moerman and Williams 2006, Gieseler, Qadota et al. 2017) (***Figure 5A***) and its
374 loss leads to paralysis, which eliminates mechanical stress on the tissue connection and
375 prevents defects in the utse-seam attachment (Gianakas, Keeley et al. 2023). To determine if
376 DDR-2 promotes integrin activity, we reduced INA-1 levels at the late L4 stage to 30% by RNAi
377 and assessed whether loss of *ddr-2* enhanced the Rup and utse-seam splitting defects (***Figure***
378 ***5—figure supplement 2D and E)***. Loss of *ddr-2* strongly enhanced the uterine prolapse defect
379 caused by RNAi-mediated knockdown of *ina-1* (***Figure 5C; Figure 5—figure supplement 2D***).
380 In addition, loss of *ddr-2* enhanced the frequency of utse-seam detachments at the late L4 stage

381 upon depletion of INA-1 (***Figure 5D***). We note that utse-seam detachments were not detected
382 upon RNAi against *ina-1* alone, likely due to incomplete knockdown at this timepoint (***Figure***
383 ***5—figure supplement 2D and E***). Together, these observations are consistent with a possible
384 role for DDR-2 in regulating integrin function to promote utse-seam connection.
385
386 To determine where integrin functions to promote utse-seam attachment, we used a previously
387 characterized dominant negative strategy, where expression of the β integrin PAT-3 lacking the
388 extracellular domain (referred to as *DN integrin*; ***Figure 5E***) inhibits endogenous integrin
389 function (Martin-Bermudo and Brown 1999, Lee, Cram et al. 2001, Hagedorn, Yashiro et al.
390 2009). We used the utse-specific *zmp-1*$^{mK50-51}$ promoter (***Figure 5—figure supplement 2F***)
391 (Hagedorn, Yashiro et al. 2009) and the seam-specific *wrt-2* promoter to disrupt integrin activity
392 in the respective tissues through the time of utse-seam tissue linkage (late L3 to young adult
393 stages, ***Figure 1D***). Expression of *DN integrin* in either the utse or the seam cells resulted in
394 utse-seam detachment at the late L4 (***Figure 5F and G***). Taken together, these findings indicate
395 that DDR-2 may promote utse-seam BM-BM adhesion in part by regulating integrin levels and
396 function.
397
398 **DDR-2 promotes vinculin localization and integrin stability at the utse-seam linkage**
399 As DDR-2 promotes integrin localization to the utse-seam BM-BM linkage and integrin activity
400 promotes utse-seam attachment, we further explored how DDR-2 may regulate integrin. Talin
401 and vinculin are core components of the integrin adhesion complex that support integrin
402 activation (Chastney, Conway et al. 2021). We thus examined endogenously tagged talin
403 (GFP::TLN-1) (Walser, Umbricht et al. 2017) and vinculin (DEB-1::mNG) localization and
404 detected both proteins at the utse-seam attachment site. Levels of each protein ramped up to
405 the late L4 and then decreased by the young adult stage, mirroring DDR-2 (***Figure 6A and B***).
406 However, loss of *ddr-2* only decreased DEB-1 levels (***Figure 6B***). Confirming a role in utse-

407 seam connection, depletion of DEB-1 by RNAi resulted in utse-seam detachment at the late L4
408 stage (***Figure 6C; Figure 6—figure supplement 1****).* These data show DDR-2 also regulates
409 vinculin levels at the utse-seam linkage and that vinculin is required for utse-seam attachment.
410
411 Integrin adhesions form stable complexes that anchor cells to ECM (Chastney, Conway et al.
412 2021). To determine whether DDR-2 regulates integrin complex stability at the site of utse-seam
413 BM-BM tissue connection, we analyzed the dynamics of INA-1 by performing Fluorescence
414 Recovery After Photobleaching (FRAP) experiments. We focused on INA-1::mNG at the late L4
415 stage when DDR-2 peaks in levels. Strikingly, loss of *ddr-2* nearly doubled the rate of recovery
416 of INA-1::mNG fluorescence signal in the bleached region 10 minutes post-bleaching as
417 compared to wild-type animals (***Figure 6D***). These observations indicate that DDR-2 stabilizes
418 the INA-1 integrin adhesion complex at the utse-seam adhesion site.
419
420 **Ras acts in the DDR-2 pathway and promotes integrin adhesion at the utse-seam linkage**
421 Vertebrate DDR2 activates multiple signaling networks, including the PI3K/Akt and Ras/Raf/Erk
422 cascades (Payne and Huang 2014, Chen, Kong et al. 2021). Notably, Ras regulates integrin
423 activity in several mammalian cell types (Zhang, Vuori et al. 1996, Conklin, Ada-Nguema et al.
424 2010, Sandri, Caccavari et al. 2012, Lilja, Zacharchenko et al. 2017). We thus hypothesized that
425 DDR-2 could promote integrin stabilization through Ras signaling. We first strongly depleted
426 LET-60 (see ***Methods***) the *C. elegans* Ras ortholog, and observed penetrant utse-seam
427 attachment defects, which were not worsened in *ddr-2* null mutant animals (***Figure 7A***). This
428 suggests that DDR-2 and LET-60/Ras function in the same pathway to mediate the utse-seam
429 connection. Next, we analyzed INA-1::mNG levels and stability after LET-60 reduction. RNAi
430 against *let-60* resulted in significantly lower INA-1 levels at the utse-seam BM-BM connection
431 site (***Figure 7B***, pre-bleach panels and ***Figure 7—figure supplement 1***). Further, like loss of

432 *ddr-2*, FRAP analysis indicated that depletion of LET-60/Ras reduced the stability of INA-1 at
433 the utse-seam linkage site (*i.e.,* there was more rapid recovery of INA-1 after photobleaching
434 (***Figure 7B***). We also generated animals harboring a gain-of-function mutation in Ras (LET-
435 $60^{G13E}$, *let-60(qy203)*) (Singh and Han 1995). Strikingly, utse-seam detachments were observed
436 in *let-60* gain-of-function animals (***Figure 7C***) and FRAP experiments revealed that INA-1 had
437 an approximately two-fold greater stability at the utse-seam BM-BM connection site (***Figure***
438 ***7D***). Collectively, these findings suggest that Ras acts downstream of DDR-2 to set the
439 appropriate levels and stability of INA-1 mediated adhesion during the formation the utse-seam
440 BM-BM tissue connection.
441

442 **Discussion**

443 To form organs such as the brain, kidney, and lung, separate tissues connect through adjoining
444 basement membrane (BM) to mediate complex functions, such as molecular barrier, blood
445 filtration, and gas exchange, respectively (Keeley and Sherwood 2019). These linkages resist
446 the independent movement of each tissue and must be strong and balanced. How cells
447 coordinate and strengthen adhesion at BM-BM linkage sites, however, is unknown. Using the *C.*
448 *elegans* utse-seam BM-BM tissue connection, we show that type IV collagen, which is the
449 molecular glue that fastens the BM-BM linkage, also activates the *C. elegans* collagen receptor
450 DDR-2 in the utse and seam tissues. DDR-2 activity synchronizes and bolsters an integrin
451 mediated adhesion to stabilize the utse-seam BM-BM tissue connection during its formation
452 (***Figure 8***).
453

454 The linkage between the multi-nucleated utse cell and epithelial seam cells allows the utse to
455 maintain the uterus within the animal during powerful egg-laying muscle contractions (Vogel and
456 Hedgecock 2001). We found that contact between the BM encased utse and seam cells occurs
457 at the time the utse cell is formed during the early L4 larval stage. This association happens just

458 prior to assembly of type IV collagen at the BM-BM linkage, a matrix component that allows the
459 linkage to resist the mechanical forces of egg-laying (Gianakas, Keeley et al. 2023). Even
460 before egg-laying, however, the utse-seam linkage resists the forces of body wall and uterine
461 muscle contractions, as defects in matrix assembly linking the BMs results in utse-seam
462 detachment during the mid L4 stage (Gianakas, Keeley et al. 2023). Through analysis of genetic
463 mutations in the *C. elegans* receptor tyrosine kinase (RTK) DDR-2, an ortholog to the two
464 vertebrate DDR receptors (DDR1 & DDR2) (Unsoeld, Park et al. 2013), we discovered that loss
465 of *ddr-2* results in utse-seam detachment beginning at the mid L4 stage. Analysis of the BM-BM
466 connecting matrix that links the BMs, which is composed of hemicentin, fibulin-1, and type IV
467 collagen, revealed it was still assembled at functional levels. This suggests that the utse and
468 seam detachment did not arise from a reduction in deposition of BM-BM linking matrix, but
469 rather a defect in tissue adhesion to the BM-BM linkage site. Our results also indicated that
470 DDR-2 functions in both the utse and seam to promote adhesion, as tissue specific expression
471 of a dominant negative DDR-2 in either tissue resulted in utse-seam detachment. Loss of DDR1
472 in mice disrupts the BM-BM connection between the podocytes and endothelial cells in the
473 kidney glomeruli and leads to defects in blood filtration (Gross, Beirowski et al. 2004),
474 suggesting a possible shared function of DDR receptors in mediating proper linkage at sites of
475 tissue connection.
476
477 In vitro studies using DDR-specific collagen binding peptides have revealed that DDRs only
478 modestly contribute directly to cell adhesion (Xu, Bihan et al. 2012). Instead, DDRs are thought
479 to initiate downstream signaling cascades that promote cell adhesion (Borza and Pozzi 2014).
480 Consistent with this notion, we observed that DDR-2::mNG was not detectable at utse and
481 seam cell surfaces when the *ddr-2* mutant attachment defect occurred between the mid to late
482 L4 stages. Instead, DDR-2 was present in early, late, and recycling endosomes of both utse and
483 seam cells. Work in a mouse osteoblast and a human kidney cell line has shown that DDR1

484 shifts from localization at the cell membrane to aggregation and internalization into early
485 endosomes within minutes of exposure to collagen (Mihai, Chotani et al. 2009). Examination of
486 the timing of DDR activation has suggested that full tyrosine receptor activation occurs within
487 the endocytic vesicles (Mihai, Chotani et al. 2009, Fu, Valiathan et al. 2013)—a signaling hub of
488 other RTKs (Murphy, Padilla et al. 2009, Villasenor, Kalaidzidis et al. 2016). We also found that
489 internalization of DDR-2 at the utse-seam connection correlated with the assembly of type IV
490 collagen at the BM-BM linkage and was dependent on type IV collagen deposition. As DDR-2 is
491 activated by ligand-induced clustering of the receptor (Juskaite, Corcoran et al. 2017, Corcoran,
492 Juskaite et al. 2019), it suggests that the BM-BM linking type IV collagen network, which is
493 specifically assembled at highly levels at the BM-BM connection, clusters and activates DDR-2
494 in the utse and seam cells to coordinate adhesion at the BM-BM linkage.
495
496 Vertebrate DDRs can promote integrin mediated cell-matrix adhesion in a variety of cell types.
497 For example, overexpression of DDR1 enhances integrin matrix adhesion in human embryonic
498 kidney cells and in human and mouse fibroblast (Xu, Bihan et al. 2012, Staudinger, Spano et al.
499 2013, Borza, Bolas et al. 2022), and high levels of DDR2 enhances integrin activation in cancer
500 associated fibroblasts in mice (Bayer, Grither et al. 2019). Several mechanisms for DDR-
501 mediated enhancement of integrin adhesion have been proposed, including increased integrin
502 surface levels and Rap1-mediated talin recruitment (Staudinger, Spano et al. 2013, Bayer,
503 Grither et al. 2019). Loss of *C. elegans rap-1* has not been reported to have a Rup/uterine
504 prolapse phenotype (Frische, Pellis-van Berkel et al. 2007) and we found that DDR-2 did not
505 promote talin recruitment to the utse-seam connection. DDR-2 did, however, increase the levels
506 of the two *C. elegans* $\alpha$ integrins—INA-1 and PAT-2—at the utse-seam linkage (Clay and
507 Sherwood 2015), as well as the integrin activating protein DEB-1/vinculin (Bays and DeMali
508 2017). Supporting a functional role for DDR-2 in promoting INA-1 mediated utse-seam
509 attachment, *ddr-2* null mutants strongly enhanced the utse-seam detachment and uterine

510 prolapse defect (Rup phenotype) of animals with reduced INA-1 function. Further, like DDR-2,
511 we found that INA-1 was expressed in the utse and seam cells and through tissue-specific
512 expression of a dominant negative integrin, we determined that integrin activity is required in
513 both tissues to promote adhesion. To understand how DDR-2 affects the strength of INA-1
514 mediated utse-seam adhesion, we performed photobleaching experiments on endogenously
515 tagged INA-1::mNG, and discovered that DDR-2 stabilizes INA-1-mediated adhesion. Through
516 genetic interaction studies, RNAi, and expression of constitutively active Ras (*C. elegans* LET-
517 60), we provide evidence that DDR-2 signals through Ras to promote INA-1 stability. Ras
518 GTPases are a key downstream mediator of DDR signaling (Chen, Kong et al. 2021). Ras has
519 been implicated in activating integrins via a poorly understood mechanism that may involve
520 integrin receptor trafficking (Zhang, Vuori et al. 1996, Conklin, Ada-Nguema et al. 2010, Sandri,
521 Caccavari et al. 2012). Interestingly, expression of the constitutively active form of Ras further
522 increased INA-1 stability at the utse-seam linkage and led to a highly penetrant utse-seam
523 detachment defect. Notably, our photobleaching experiments showed that there was a wide
524 range of integrin stability at the utse-seam attachment site in wild-type animals, likely reflecting
525 low to high adhesion strength. However, Ras activation narrowed integrin to within a high
526 stability range (i.e. high adhesion strength), while *ddr-2* loss as well as Ras reduction shifted
527 integrin towards a narrow, low stability range (low adhesion strength). Together, our
528 observations suggest that DDR-2 signaling through Ras facilitates an increased range of
529 integrin adhesion at the utse-seam connection, which is required to maintain the utse-seam
530 linkage.
531
532 The utse-seam adhesion at the BM-BM tissue linkage is built in the L4 larval stage and then
533 maintained in the adult to support egg-laying (Gianakas, Keeley et al. 2023). Our evidence
534 indicates that DDR-2 activity is highest and perhaps only required between the mid and late L4
535 larval stages (~four-hour period), as the utse-seam detachment defect peaked by the mid-to-

536 late L4 stage and did not worsen at the late L4 and young adult stages. This timing aligns with a
537 spike in DDR-2 levels in the utse and seam cells and is also when DDR-2 most strongly
538 promoted INA-1 integrin and vinculin levels at the utse-seam linkage. It is possible that DDR-2 is
539 specifically required between the mid and late L4 stages to facilitate a wide range of integrin
540 adhesion. This could adjust the cell-matrix adhesion strength as the BM-BM connecting matrix
541 assembles, strengthens, and changes composition during this time window, shifting from a
542 hemicentin and fibulin-rich to a type IV collagen-dominated matrix (Gianakas, Keeley et al.
543 2023). Alternatively, a range of integrin adhesion strength may be required to maintain the utse-
544 seam linkage, while allowing the utse and seam to undergo morphogenetic changes to form the
545 tongue (utse) and groove (seam) morphology that secures the tissue linkage. Collectively, our
546 findings support the idea that although the ligands for DDRs are stable collagen molecules,
547 DDRs can function as dynamic sensors of the external environment, allowing cells and tissues
548 to coordinate their activities with changes to the extracellular surroundings.
549
550
551
552
553
554
555
556
557
558
559
560

561 **Materials and Methods**

562 **Key resources table**

| Reagent type (species) or resource | Designation | Source or reference | Identifiers | Additional information |
|---|---|---|---|---|
| Strain, strain background (*C. elegans*) | NK2617 | (Gianakas, Keeley et al. 2023) | | *qyIs23 [cdh-3p::mCh::PH]* II*; lqIs80 [scmp::GFP::CAAX]* IV |
| Strain, strain background (*C. elegans*) | N2 | Caenorhabditis Genetics Center (CGC) | | Wild type (ancestral) |
| Strain, strain background (*C. elegans*) | RB970 | | | *ddr-1(ok874)* X |
| Strain, strain background (*C. elegans*) | VH1387 | (Unsoeld, Park et al. 2013) | | *ddr-1(tm382)* X |
| Strain, strain background (*C. elegans*) | RB788 | | | *ddr-2(ok574)* X |
| Strain, strain background (*C. elegans*) | VH1383 | (Unsoeld, Park et al. 2013) | | *ddr-2(tm797)* X |

| | | | | |
|---|---|---|---|---|
| Strain, strain background (*C. elegans*) | NK2511 | This study | | *ddr-2(qy64)* X |
| Strain, strain background (*C. elegans*) | NK2655 | This study | | *qyIs23 [cdh-3p::mCh::PH]* II; *lqIs80 [scmp::GFP::CAAX]* IV; *ddr-2(qy64)* X |
| Strain, strain background (*C. elegans*) | NK2640 | This study | | *qy91 [nas-22p::2xmKate2::PH*] II; *lqIs80* [*scmp::GFP::CAAX*] IV |
| Strain, strain background (*C. elegans*) | NK2682 | This study | | *qy91 [nas-22p::2xmKate2::PH]* II; *lqIs80 [scmp::GFP::CAAX]* IV; *ddr-2(qy64)* X |
| Strain, strain background (*C. elegans*) | | This study | | *qy44 [ddr-2::mNG]* X; *qyEx605 [scmp::2xmKate2:PH]* |

| | | | | |
|---|---|---|---|---|
| Strain, strain background (*C. elegans*) | NK2620 | This study | | *qyIs23 [cdh-3p::mCh::PH]* II*; qy44 [ddr-2::mNG]* X |
| Strain, strain background (*C. elegans*) | NK2763 | This study | | *qyIs256 [cdh-3p::mCherry::rab-5]* ?; *qy44 [ddr-2::mNG*] X |
| Strain, strain background (*C. elegans*) | NK2766 | This study | | *qyIs252 [cdh-3p::mCherry::rab-7]* ?; *qy44 [ddr-2::mNG*] X |
| Strain, strain background (*C. elegans*) | NK2769 | This study | | *qyIs205 [cdh-3p::mCherry::rab-11]* ?; *qy44 [ddr-2::mNG*] X |
| Strain, strain background (*C. elegans*) | NK2901 | This study | | *qy188 [scmp::mKate2::rab-5]* I; *qy44 [ddr-2::mNG*] X |
| Strain, strain background (*C. elegans*) | NK2926 | This study | | *qy91 [nas-22p::2xmKate2::PH*] II; *IqIs80* [*scmp::GFP::CAAX*] IV; *ddr-2(ok574)* X |

| | | | | |
|---|---|---|---|---|
| Strain, strain background (*C. elegans*) | NK2705 | (Jayadev, Morais et al. 2022) | | *qy118 [col-99::mNG (internal tag)]* IV |
| Strain, strain background (*C. elegans*) | NK2322 | (Keeley, Hastie et al. 2020) | | *qy22 [cle-1::mNG]* I |
| Strain, strain background (*C. elegans*) | NK2326 | (Keeley, Hastie et al. 2020) | | *qy24 [emb-9::mNG (internal tag)]* III |
| Strain, strain background (*C. elegans*) | NK2830 | This study | | *qy166 [cdh-3p::dominant negative ddr-2::mNG]* I; *qy91 [nas-22p::2xmKate2::PH]* II; *heIs63 [wrt-2p::GFP::PH + wrt-2p::GFP::H2B + lin-48p:mCherry]* V |
| Strain, strain background (*C. elegans*) | NK2848 | This study | | *qy175 [scmp::dominant negative ddr-2::mKate2]* I; *qy91 [nas-22p::2xmKate2::PH]* |

| | | | | |
|---|---|---|---|---|
| | | | | II; *heIs63 [wrt-2p::GFP::PH + wrt-2p::GFP::H2B + lin-48p:mCherry]* V |
| Strain, strain background (*C. elegans*) | NK2585 | (Jayadev, Morais et al. 2022) | | *qy83 [emb-9::mRuby2 (internal tag)]* III |
| Strain, strain background (*C. elegans*) | NK2422 | (Keeley, Hastie et al. 2020) | | *qy33 [him-4::mNG]* X |
| Strain, strain background (*C. elegans*) | NK2324 | (Jayadev, Chi et al. 2019) | | *qy23 [ina-1::mNG]* III |
| Strain, strain background (*C. elegans*) | NK2479 | (Jayadev, Chi et al. 2019) | | *qy49 [pat-2::2xmNG]* III |
| Strain, strain background (*C. elegans*) | NK2825 | This study | | *qy23 [ina-1::mNG]* III; *ddr-2(qy64)* X |
| Strain, strain background (*C. elegans*) | NK2858 | This study | | *qy49 [pat-2::2xmNG]* III; *ddr-2(qy64)* X |
| Strain, strain background (*C. elegans*) | NK2804 | This study | | *qyIs23 [cdh-3p::mCh::PH]* II; *heIs63 [wrt-* |

| | | | | |
|---|---|---|---|---|
| | | | | *2p::GFP::PH + wrt-2p::GFP::H2B + lin-48p:mCherry]* V |
| Strain, strain background (*C. elegans*) | NK2824 | This study | | *qyIs23 [cdh-3p::mCh::PH]* II; *qyIs15 [zmp-1$^{mk50-51}$p::dominant negative integrin b-pat-3]* IV;*heIs63 [wrt-2p::GFP::PH + wrt-2p::GFP::H2B + lin-48p:mCherry]* V |
| Strain, strain background (*C. elegans*) | NK2934 | This study | | *qy91 [nas-22p::2xmKate2::PH*] II; *unc-119(ed4)* III; *IqIs80* [*scmp::GFP::CAAX*] IV; *qyEx604 [wrt-2p::dominant negative integrin b-pat-3 + unc-119(+)]* |
| Strain, strain background (*C. elegans*) | NK2579 | (Keeley, Hastie et al. 2020) | | *qy62 [mNG::fbl-1] IV* |

| | | | | |
|---|---|---|---|---|
| Strain, strain background (*C. elegans*) | NK932 | (Kelley, Chi et al. 2019) | | *qyIs190 [zmp-4p::zmp-4::GFP]* |
| Strain, strain background (*C. elegans*) | NK268 | (Hagedorn, Yashiro et al. 2009) | | *qyIs17 [zmp-1$^{mk50-51}$p mCherry]* |
| Strain, strain background (*C. elegans*) | AH3437 | (Walser, Umbricht et al. 2017) | | *zh117 [GFP::tln-1]* I |
| Strain, strain background (*C. elegans*) | NK2478 | This study | | *qy48 [deb-1::mNG]* IV |
| Strain, strain background (*C. elegans*) | NK2854 | This study | | *zh117 [GFP::tln-1]* I; *ddr-2(qy64)* X |
| Strain, strain background (*C. elegans*) | NK2860 | This study | | *qy48 [deb-1::mNG]* IV; *ddr-2(qy64)* X |
| Strain, strain background (*C. elegans*) | NK2944 | This study | | *qy91 [nas-22p::2xmKate2::PH*] II; *lqIs80* [*scmp::GFP::CAAX*] IV; *let-60(qy203)* IV |

| | | | | |
|---|---|---|---|---|
| Strain, strain background (*C. elegans*) | NK2957 | This study | | *qy23 [ina-1::mNG]* III; *let-60(qy203)* IV |
| Strain, strain background (*E. coli*) | *emb-9* RNAi | (Kamath and Ahringer 2003) | | Clone from Ahringer library (L4440 vector backbone) |
| Strain, strain background (*E. coli*) | *col-99* RNAi | (Rual, Ceron et al. 2004) | | Clone from Vidal library (L4440 vector backbone) |
| Strain, strain background (*E. coli*) | *cle-1* RNAi | (Rual, Ceron et al. 2004) | | Clone from Vidal library (L4440 vector backbone) |
| Strain, strain background (*E. coli*) | *ina-1* RNAi | (Rual, Ceron et al. 2004) | | Clone from Vidal library (L4440 vector backbone) |
| Strain, strain background (*E. coli*) | *let-60* RNAi | (Rual, Ceron et al. 2004) | | Clone from Vidal library (L4440 vector backbone) |
| Strain, strain background (*E. coli*) | *deb-1* RNAi | (Rual, Ceron et al. 2004) | | Clone from Vidal library (L4440 vector backbone) |
| Strain, strain background (*E. coli*) | *him-4* RNAi | (Gianakas, Keeley et al. 2023) | | T444t vector backbone |

| | | | | |
|---|---|---|---|---|
| Strain, strain background (*E. coli*) | *ddr-2* RNAi | This study | | T444t vector backbone |
| Sequence-based reagent | *ddr-2* knockout (*ddr-2(qy64)*) sgRNA 1 | This study | | ATCCTGACATAGA TGAGCGT |
| Sequence-based reagent | *ddr-2* knockout (*ddr-2(qy64)*) sgRNA 2 | This study | | GTCATTGGTGCAC ACTTCTC |
| Sequence-based reagent | *ddr-2* knockout (*ddr-2(qy64)*) sgRNA 3 | This study | | AAGTGTGCACCAA TGACTGG |
| Sequence-based reagent | *deb-1::mNG* (*deb-1(qy48)*) sgRNA 1 | This study | | AGTTGGACCACAT TGGCTTT |
| Sequence-based reagent | *deb-1::mNG* (*deb-1(qy48)*) sgRNA 2 | This study | | ATTTAGAAGTTGG ACCACAT |
| Sequence-based reagent | *let-60* gain-of-function (*let-60(qy203)*) sgRNA 1 | This study | | CTTGTGGTAGTTG GAGATGG |
| Sequence-based reagent | Primer *ddr-2(qy64)* homology arm forward | This study | | TTTTCAGAGTCTC CGACGCTCATCTA |

| | | | | |
|---|---|---|---|---|
| Sequence-based reagent | Primer *ddr-2(qy64)* homology arm reverse | This study | | TAAATATTATTCTG AGAATATA |
| Sequence-based reagent | Primer *ddr-2(qy64)* genotyping forward | This study | | TGGTAATTGATGA GAGGGTG |
| Sequence-based reagent | Primer *ddr-2(qy64)* genotyping reverse | This study | | TGTCGTTTCGACA CCGGCAA 1.8 kb band |
| | Primer *let-60(qy203)* homology arm forward | This study | | ATGACGGAGTACA AGCTTGTGGTAGT TGGAGATGGAGA AGT |
| | Primer *let-60(qy203)* homology arm reverse | This study | | TACCCTTTTCTGA AAAAAGACGC |
| Sequence-based reagent | Primer *nas-22* promoter forward | This study | | TCAAAGCGTCAAG CTTTACG |

| | | | | |
|---|---|---|---|---|
| Sequence-based reagent | Primer *nas-22* promoter reverse | This study | | TTTTCTGTCTACAAGGACTGTGC |
| Sequence-based reagent | Primer *scm* promoter forward | (Chapman, Li et al. 2008) | | AACCTCCACCAGATGGTTGGCG |
| Sequence-based reagent | Primer *scm* promoter reverse | (Chapman, Li et al. 2008) | | CCCGGGGATCCGTCCACTCT |
| Sequence-based reagent | Primer *cdh-3* promoter forward | This study | | CTAGAGCATGATGTCCTTAC |
| Sequence-based reagent | Primer *cdh-3* promoter reverse | This study | | CAAAACGGACCGACCGTCCC |
| Sequence-based reagent | Primer *dominant negative ddr-2* forward | This study | | ATGAAGTTGCTGCTGTATCT |
| Sequence-based reagent | Primer *dominant negative ddr-2* reverse | This study | | TCTGCTCACGCAAATCAACT |

| | | | | |
|---|---|---|---|---|
| Sequence-based reagent | Primer *wrt-2* promoter forward | This study | | TCAGAACTCTAATACTTACT |
| Sequence-based reagent | Primer *wrt-2* promoter reverse | This study | | CCGAGAAACAATTGGCAGGT |
| Sequence-based reagent | Primer *dominant negative integrin b pat-3* forward | (Hagedorn, Yashiro et al. 2009) | | TCTAGAGGATCCCGGGGAT |
| Sequence-based reagent | Primer *dominant negative integrin b pat-3* reverse | (Hagedorn, Yashiro et al. 2009) | | ATTTAGTTGGCTTTTCCAGC |
| Sequence-based reagent | Primer *ddr-2* RNAi forward | This study | | ATGAAGTTGCTGCTGTATCT |
| Sequence-based reagent | Primer *ddr-2* RNAi reverse | This study | | ATGAATATGAGGAGAAGTGTGC |
| Recombinant DNA reagent | Plasmid: pCFJ352 | Addgene | RRID: Addgene_30539 | sgRNA targeting MosSCI insertion |

| | | | | |
|---|---|---|---|---|
| | | | | site on Chr I, from Erik Jorgensen |
| Recombinant DNA reagent | Plasmid: pDD122 | (Dickinson, Ward et al. 2013) | RRID: Addgene_47550 | sgRNA targeting MosSCI insertion site on Chr II |
| | Plasmid: pAP087 | (Pani and Goldstein 2018) | | starter SEC repair template plasmid for single copy insertion at the ttTi5605 site on chromosome II |
| Recombinant DNA reagent | Plasmid: pAP088 | (Pani and Goldstein 2018) | | starter SEC repair template plasmid for single copy insertion at the ttTi4348 site on chromosome I |
| Chemical compound, drug | Ampicillin | Sigma-Aldrich | #A0166 | |
| Chemical compound, drug | Isopropyl β-D-1-thiogalactopyranoside | Sigma-Aldrich | #I6758 | |
| Chemical compound, drug | Hygromycin B | Sigma-Aldrich | #H3274 | |
| Chemical compound, drug | Sodium azide | Sigma-Aldrich | #S2002 | |

| | | | | |
|---|---|---|---|---|
| Chemical compound, drug | Levamisole | Sigma-Aldrich | #L9756 | |
| Software, algorithm | µManager v.1.4.23 | | | |
| Software, algorithm | Zen Black | | | |
| Software, algorithm | Fiji/ImageJ | | | |
| Software, algorithm | GraphPad Prism v9 | | | |

563

564 ***C. elegans* culture and strains**

565 *C. elegans* strains used in this study are listed in the ***Key resources table***. Worms were reared
566 on nematode growth medium plates seeded with OP50 *Escherichia coli* at 16°C, 18°C, or 20°C
567 according to standard procedures (Stiernagle 2006). We used *C. elegans* vulval development to
568 accurately stage animals through the morphogenesis of the utse-seam connection (late L3 to
569 young adult stage) (Mok, Sternberg et al. 2015).

570

571 **Generation of genome-edited strains**

572 To generate the genome-edited mNeonGreen (mNG) knock-in allele for *deb-1* (*qy48*), we used
573 CRISPR/Cas9 genome editing with a self-excising cassette (SEC) for drug selection
574 (hygromycin treatment) as described previously (Dickinson, Ward et al. 2013, Keeley, Hastie et
575 al. 2020). An 18 amino acid flexible linker attached to the mNG fluorophore was inserted in
576 frame and directly upstream of the stop codon. sgRNA sequences directing Cas9 cleavage near
577 the C-terminus are provided in the ***Key resources table***.

578

579 The *ddr-2* knockout allele *ddr-2(qy64)*, an 8615 bp deletion corresponding to the coding
580 sequence of DDR-2, was also generated with the SEC CRISPR method detailed above with one
581 modification—we generated a new starter repair plasmid lacking the fluorescent tag. Primers
582 used to amplify homology arms, sgRNA sequences to direct Cas9 cleavage, and genotyping
583 primers used to verify genome-edited knockout animals are provided in the ***Key resources***
584 ***table***.
585
586 For the LET-60$^{G13E}$ gain-of function mutation, *let-60(qy203)*, we used the same strategy as the
587 *ddr-2* knockout allele. The point mutation was incorporated into the primer for homology arm
588 amplification. Note that this mutation is identical to the *let-60(n1046)* allele.
589
590 **Generation of transgenic strains**
591 For the utse marker *qy91 [nas-22p::2xmKate2::pH]*, we generated a single-copy transgene
592 inserted into the ttTi5605 transposon insertion on chromosome II (Frokjaer-Jensen, Davis et al.
593 2012) using the SEC CRISPR method detailed above. A 2 kb *nas-22* promoter, two tandem
594 mKate2 fluorophores attached to a PH domain, and an *unc-54* 3' UTR fragment were ligated in
595 order via Gibson assembly into the pAP087 starter repair plasmid containing homology arms for
596 the ttTi5605 site. The sgRNA directing Cas9 cleavage near this region is contained in the
597 pDD122 vector.
598
599 To express mKate2-tagged RAB-5 in the seam, we generated a single-copy transgene inserted
600 into the ttTi4348 transposon insertion site on chromosome I (Frokjaer-Jensen, Davis et al. 2012)
601 using SEC CRISPR. Briefly, the scm promoter, mKate2 fluorophore, rab-5 genomic sequence,
602 and *unc-54* 3' UTR were Gibson assembled in order into the pAP088 starter repair plasmid
603 containing homology arms for the ttTi4348 site. The sgRNA directing Cas9 cleavage near this
604 region is contained in the pCFJ352 vector.

605

606 For tissue-specific expression of dominant negative (DN) DDR-2 in the utse or seam, we also
607 generated single-copy transgenes inserted into the ttTi4348 site. For utse expression, the
608 following fragments were Gibson assembled in order into pAP088: a 1.5kb *cdh-3* promoter
609 fragment, *DN ddr-2*, mNG fluorophore, and *unc-54* 3' UTR. Expression in transgenic animals
610 was verified by assessing mNG fluorescence. For seam expression, the following fragments
611 were Gibson assembled in order into pAP088: the *scm* promoter fragment, *DN ddr-2*, and
612 mKate2 fluorophore. Expression in transgenic animals was verified by assessing mKate2
613 fluorescence.

614

615 The seam cell marker *qyEx605 [scmp::2xmKate2::PH]* was built by Gibson assembling a 1.3 kb
616 *scm* promoter fragment, a fragment with two tandem mKate2 fluorophores attached to the PH
617 domain, and *unc-54* 3' UTR fragment in order. The construct was expressed as
618 extrachromosomal arrays as described previously (Yochem and Herman 2003).

619

620 To build the construct for *DN integrin* expressed in the seam, we first amplified the *DN integrin*
621 fragment from animals harboring the *qyIs15* allele (see ***Key resources table***). The *DN integrin*
622 fragment is composed of a *pes-10* enhancer element, the *ost-1* signal peptide, the *pat-3* β-tail
623 fragment, and *unc-54* 3' UTR as described previously (Lee Cram et al. 2001). The *DN integrin*
624 fragment was fused to a 1.3 kb *wrt-2* promoter by PCR. The construct was expressed
625 extrachromosomally.

626

627 **RNAi**

628 All RNAi constructs except for *ddr-2* RNAi were obtained from the Ahringer and Vidal RNAi
629 libraries (Kamath and Ahringer 2003, Rual, Ceron et al. 2004) or generated previously
630 (Gianakas, Keeley et al. 2023). For the *ddr-2* clone, a ~2.4 kb cDNA fragment corresponding to

631 the longest *ddr-2* transcript was amplified by PCR and inserted into the T444t vector as
632 described previously (Gianakas et al 2023). RNAi experiments were performed using the
633 feeding method (Timmons, Court et al. 2001) according to previously detailed protocols
634 (Jayadev, Chi et al. 2019, Gianakas, Keeley et al. 2023). For experiments assessing the utse-
635 seam connection, RNAi was initiated in synchronized L1 larvae and animals were examined at
636 the late L4 stage (~ 44 h treatment). For examination of uterine prolapse, RNAi was performed
637 from the L1 through adulthood (~ 120 h treatment). For depletion of hemicentin initiated at the
638 early L4 stage, synchronized L1 worm were grown on control RNAi for ~ 38 h to the early L4,
639 and then transferred onto *him-4* RNAi to the late L4 (~5-6 h treatment). We verified knockdown
640 efficiencies for all RNAi experiments except for *let-60* RNAi by including a control with the
641 relevant fluorescent tagged target protein, achieving between ~75 to 100% reduction. We
642 verified *let-60* RNAi knockdown efficiency by plate level assessment of brood size, which was
643 strongly reduced compared to control animals, as previously reported (Ceron, Rual et al. 2007).
644

645 **Microscopy and image processing**

646 All fluorescence images (except for photobleaching experiments) were acquired at 20°C on
647 Zeiss Axio Imager A1 microscopes controlled by the μManager software v.1.4.23 or v.2.0.1
648 (Edelstein, Amodaj et al. 2010), equipped with a Hamamatsu ImagEM electron multiplying
649 charge-coupled device camera or an Orca-Fusion scientific complementary metal oxide
650 semiconductor camera, Zeiss 40x and 100x Plan Apochromat (1.4 numerical aperture) oil
651 immersion objectives, Yokogawa CSU-10 spinning disc confocal scan heads, and 488 nm, 505
652 nm, and 561 nm laser lines. Worms were mounted on 5% noble agar pads containing 0.01M
653 sodium azide for imaging.
654

655 For photobleaching experiments, images were acquired at 20°C on a Zeiss 880 single-point
656 scanning confocal attached to a Zeiss Axio Observer Z1 microscope, with a Marzhauser linearly

657 encoded stage, a 40x Plan Neofluar (1.3 numerical aperture) oil immersion objective, and a 488
658 nm laser line. Worms were anesthetized by soaking in 5 mM levamisole in M9 buffer for 15 min
659 and then transferred to 4% noble agar pads. Coverslips were then placed and sealed on top
660 with valap (equal weight Vaseline, lanolin, and paraffin) and flooded with 5 mM levamisole.
661 Coverslip sealing kept the animals hydrated during the experimental timeframe, ensuring
662 accurate imaging of endogenous protein dynamics (detailed in (Kelley, Wang et al. 2017)). A
663 rectangle region within one arm of the BM-BM connection BLINK was photobleached using 30
664 iterations of simultaneous 405 nm and 488 nm excitation at 100% laser power for a total
665 bleaching time of 1.5 seconds. Worms were imaged prior and immediately following bleaching,
666 and then again 10 min later.
667
668 Brightfield images of worms were acquired at 20°C on a Zeiss Axio Zoom V16 stereo
669 fluorescence microscope controlled by Zen 3.2 software, equipped with an Axiocam digital
670 camera and a 3x objective. Worms were imaged without immobilization.
671
672 To image the utse and seam cells ventrally, we manually oriented animals in the ventral
673 orientation (Kelley, Wang et al. 2017) and acquired z-stacks at 0.37 μm intervals, capturing the
674 entire H-shaped structure of the utse and the seam cells flanking both sides of the utse at 100x
675 magnification. Ventral views of the utse and seam shown in figures are maximum intensity
676 projections of these z-stacks. 3D isosurface renderings of the utse and seam cells shown in
677 ***Figure 2D*** were generated with Imaris 7.4 software (Bitplane). We acquired lateral z-stacks at
678 0.37 μm intervals to fully capture the superficial half of the utse-seam attachment.
679
680 For lateral imaging of DDR-2::mNG together with the utse, seam cells, or endosome markers
681 expressed in the utse or seam, we acquired z-stacks at 0.37 μm intervals to capture as much of
682 each tissue that was in focus superficially at 40x magnification. Images shown in figures are

683 single slices where DDR-2 was sharply in focus within the tissue of interest. The same
684 parameters were used for imaging INA-1::mNG and PAT-2::mNG in the utse and seam. Images
685 in ***Figure 5A*** correspond to the z-slices where INA-1 and PAT-2 were most in focus at the BM-
686 BM connection region. In ***Figure 5—figure supplement 2A and B***, images shown are sum
687 projections of the seam or utse regions.
688
689 To image DDR-2::mNG specifically at the utse-seam attachment site, we acquired lateral z-
690 stacks at 0.37 µm intervals capturing both the surface of the utse and the seam cells. We used
691 a utse cell marker as a reference to accurately capture this region (see also schematic in ***Figure***
692 ***3A***). Images shown in ***Figure 4*** are sum projections of these z-stacks.
693
694 For lateral imaging of respective tagged proteins at the BM-BM connection region, we acquired
695 single slices (40x magnification) at the middle focal plane where the BM-BM connection signal
696 was sharply in focus. All images were process in Fiji 2.0 (Schindelin, Arganda-Carreras et al.
697 2012).
698
699 **Image analysis and quantification**
700 To assess utse-seam detachment, we used maximum intensity projections of the utse and
701 seam viewed ventrally as detailed above. We defined utse-seam detachment as any gap in the
702 utse-seam attachment of at least 4 square pixels in area. We preferred the ventral view over 3D
703 rendering for this metric as gaps were variable in size and location (typically occurring in one or
704 two arms of the utse on opposite sides). The ventral projections allowed us to reliably examine
705 all four arms of the utse and whether they were in contact with the seam from animal to animal.
706 The visual representation of a gap in a ventral maximum projection is an underestimate of the
707 true size of the detachment, as the tongue-in-groove association of the utse and seam can only
708 be seen in a 3D surface rendering of the utse and seam viewed from the side. We thus used a

709 binary scoring system (animals with or without utse-seam detachments) instead of quantifying
710 the size of the detached region. We note that ventral imaging of the utse and seam sometimes
711 results in small utse-seam detachments as we manually orient the animals on the slide. To
712 control for this, we acquired large datasets (at least 40 animals examined) for every control
713 strain we used to visualize the utse-seam attachment with. We found that small detachments
714 related to ventral imaging occurred in ~8-12% of animals, depending on the genetic
715 background. All datasets shown in figures have been normalized to account for this.
716
717 All quantifications of mean fluorescence intensity were done on raw images in Fiji 2.0. We drew
718 ~5-pixel long and 2-pixel wide linescans to obtain raw values of mean fluorescence intensity.
719 For measurement within the BM-BM connection region, we positioned the linescan within the
720 arm that was most in focus. Other regions where linescans were performed are indicated in
721 figures. Background intensity values were obtained with similar linescans in adjacent regions
722 with no visible fluorescence signal. Note that we used two tandem mNG fluorophores to
723 visualize PAT-2 at the utse-seam attachment site (PAT-2::2xmNG) as it was present at very low
724 levels. We imaged PAT-2::mNG and PAT-2::2xmNG in this region at the same exposure and
725 found that the latter was approximately two times brighter (PAT-2::2xmNG mean fluorescence
726 intensity 3941 ± 847 A.U., PAT-2::mNG 2037 ± 465 A.U., n = 10 animals examined each).
727 Taken together with quantifications in ***Figure 5B***, INA-1 is thus likely present at six-fold higher
728 levels than PAT-2 at the utse-seam attachment site. For additional quantification related to
729 FRAP, see below.
730
731 For FRAP analysis, we measured mean fluorescence intensity within the bleached region. In
732 addition, we performed an equivalent linescan within the unbleached arm at the BM-BM
733 connection to calculate a bleach correction factor to account for general photobleaching during
734 image acquisition across the duration of the experiment, as previously described (Gianakas,

735 Keeley et al. 2023). Briefly, the background-corrected fluorescence intensity measurement on
736 the side of the BM-BM connection where FRAP was not performed at the 10 min post-bleach
737 timepoint was divided by the respective value at the pre-bleach timepoint to obtain the bleach
738 correction factor. Fluorescence intensity measurements at the pre-bleach and post-bleach
739 timepoints on the side of the BM-BM connection where FRAP was performed were then
740 multiplied by the respective bleach correction factor to normalize these values to the 10 min
741 post-bleach fluorescence intensity measurement in the same region.
742
743 To count the number of DDR-2 punctae at the site of utse-seam attachment, we used sum
744 projections of DDR-2::mNG capturing the surface of the utse and seam (described earlier). We
745 restricted measurements to the utse-seam connection corresponding to one utse arm.
746 Brightness and contrast was then adjusted to manually count individual punctae, as DDR-2
747 punctae showed a large variance in size and fluorescence intensity. Note that in the type IV
748 collagen depletion condition, we only counted discrete puncta and did not include the large cell
749 surface accumulation of DDR-2 in the analysis.
750
751 To determine co-localization of DDR-2 with markers of endocytic vesicles, we also used a
752 manual approach due to the large variability of the size and fluorescence intensity of punctae.
753 We selected a single slice where the utse or the seam was sharply in focus, and restricted
754 measurements to a single utse arm or a region of the seam corresponding to a single utse arm.
755 For each animal, the number, and positions of DDR-2 punctae were noted and compared to the
756 respective endosome marker (RAB-5, RAB-7, or RAB-11). If a DDR-2 puncta physically
757 overlapped with or was in contact with an endosome punctum, it was classified as one that co-
758 localized with the endosomal marker. We then calculated the percentage overlap of DDR-2
759 punctae with the vesicle marker for each animal (corresponding to each data point within
760 boxplots in ***Figure 3—figure supplement 1B and C***).

761

762 **Scoring of uterine prolapse**

763 Synchronized L1 larvae were plated (~20 animals per plate) and after 24 h, the exact number of
764 worms on each plate was recorded. Plates were then visually screened for ruptured worms
765 (uterine prolapse) every 24 h, up to 120 h post L1 plating. Ruptured animals were scored and
766 removed from plates to avoid double counting and after 120 h, the percentage of animals with
767 uterine prolapse was calculated. At least 50 animals were screened for every experiment.

768

769 **Illustrations of utse-seam tissue connection**

770 For schematics in Figure 1A and Figure 8, model protein sizing was scaled according to
771 previously generated models (Keeley, Hastie et al. 2020). We sized hemicentin, fibulin, type IV
772 collagen, integrin, and DDR-2. We also approximated the span of the basement membranes of
773 the utse and seam cells (~50 nm each), as well as the BM-BM connecting matrix (~200 nm),
774 based on electron microscopy of the utse-seam attachment (Vogel and Hedgecock 2001).

775

776 **Statistical analysis**

777 Statistical analysis was performed in GraphPad Prism 9. Normality of datasets was assessed
778 using the D'Agostino-Pearson normality test. We used parametric tests for datasets that
779 followed a Gaussian distribution and non-parametric tests for those that did not. For
780 comparisons of means between two populations, we used either an unpaired two-tailed
781 Student's *t* test or a Mann-Whitney *U* test. For comparisons of means between three or more
782 populations, we performed either a one-way ANOVA followed by post hoc Dunnett's test or
783 Kruskal-Wallis *H* test with post hoc Dunn's test. For comparisons between two categorical
784 variables, we used the Fisher's exact test. All graphs were prepared in GraphPad Prism. Figure
785 legends indicate sample sizes, statistical tests used, and *P* values.

786

## Data availability

All data generated in this study are included in the manuscript and supporting files.


## Acknowledgements

We would like to thank C. Borza, A. Pozzi, B. Hoffman, and D. Reiner for helpful discussions, C. Gianakas for comments on the manuscript, and M. Boxem and H. Hutter for strains. Some strains were provided by the CGC, which is funded by NIH Office of Research Infrastructure Programs (P40 OD010440). S.G.P. was supported by graduate research fellowship NICHD F31 HD97901. This work was supported by R35GM118049, R21OD028766, and R21OD032430 to D.R.S.


## Additional Information


### Funding

| Funder | Grant reference number | Author |
|---|---|---|
| National Institutes of Health | R35GM118049 | David R. Sherwood |
| National Institutes of Health | R21OD028766 | David R. Sherwood |
| National Institutes of Health | R21OD032430 | David R. Sherwood |
| National Institute of Child Health and Human Development | F31 HD97901 | Sara G. Payne |

## Author Contributions

Kieop Park, conceptualization, data curation, formal analysis, investigation, visualization, methodology, writing-original draft; Ranjay Jayadev, conceptualization, data curation, formal analysis, investigation, visualization, methodology, writing-original draft; Sara G. Payne, Conceptualization, data curation, formal analysis, investigation, visualization, methodology, writing-original draft, funding acquisition; Isabel W. Kenny-Ganzert, investigation, methodology; Qiuyi Chi, investigation, methodology; Daniel S. Costa, methodology; William Ramos-Lewis, investigation, methodology; Siddharthan Balachandar Thendral, visualization; David R. Sherwood, supervision, writing-original draft, funding acquisition, project administration.

## Competing Interests

No competing interests declared for all authors

## Author ORCID

Kieop Park https://orcid.org/0000-0002-6380-4730

Ranjay Jayadev https://orcid.org/0000-0003-0465-0337

Sara G. Payne https://orcid.org/0000-0002-3572-9112

Isabel Kenny-Ganzert https://orcid.org/0000-0001-6306-4472

Qiuyi Chi https://orcid.org/0000-0003-1297-4163

Daniel S. Costa https://orcid.org/0000-0003-2179-8800

Will Ramos-Lewis https://orcid.org/0000-0002-4627-4571

Siddharthan Balachandar Thendral https://orcid.org/0000-0002-4674-7033

David R Sherwood https://orcid.org/0000-0002-4448-6917

## References


Abrahamson, D. R. (1985). "Origin of the glomerular basement membrane visualized after in vivo labeling of laminin in newborn rat kidneys." J Cell Biol **100**(6): 1988-2000.

Altincicek, B., M. Fischer, M. Fischer, K. Luersen, M. Boll, U. Wenzel and A. Vilcinskas (2010). "Role of matrix metalloproteinase ZMP-2 in pathogen resistance and development in Caenorhabditis elegans." Dev Comp Immunol **34**(11): 1160-1169.

Bayer, S. V., W. R. Grither, A. Brenot, P. Y. Hwang, C. E. Barcus, M. Ernst, P. Pence, C. Walter, A. Pathak and G. D. Longmore (2019). "DDR2 controls breast tumor stiffness and metastasis by regulating integrin mediated mechanotransduction in CAFs." Elife **8**.

Bays, J. L. and K. A. DeMali (2017). "Vinculin in cell-cell and cell-matrix adhesions." Cell Mol Life Sci **74**(16): 2999-3009.

Bernadskaya, Y. Y., S. Brahmbhatt, S. E. Gline, W. Wang and L. Christiaen (2019). "Discoidin-domain receptor coordinates cell-matrix adhesion and collective polarity in migratory cardiopharyngeal progenitors." Nat Commun **10**(1): 57.

Borza, C. M., G. Bolas, X. Zhang, M. B. Browning Monroe, M. Z. Zhang, J. Meiler, M. J. Skwark, R. C. Harris, L. A. Lapierre, J. R. Goldenring, M. Hook, J. Rivera, K. L. Brown, B. Leitinger, M. J. Tyska, M. Moser, R. T. Bottcher, R. Zent and A. Pozzi (2022). "The Collagen Receptor Discoidin Domain Receptor 1b Enhances Integrin beta1-Mediated Cell Migration by Interacting With Talin and Promoting Rac1 Activation." Front Cell Dev Biol **10**: 836797.

Borza, C. M. and A. Pozzi (2014). "Discoidin domain receptors in disease." Matrix Biol **34**: 185-192.

Brown, K. L., C. F. Cummings, R. M. Vanacore and B. G. Hudson (2017). "Building collagen IV smart scaffolds on the outside of cells." Protein Sci **26**(11): 2151-2161.

Brown, N. H. (2011). "Extracellular matrix in development: insights from mechanisms conserved between invertebrates and vertebrates." Cold Spring Harb Perspect Biol **3**(12).

Carney, T. J., N. M. Feitosa, C. Sonntag, K. Slanchev, J. Kluger, D. Kiyozumi, J. M. Gebauer, J. Coffin Talbot, C. B. Kimmel, K. Sekiguchi, R. Wagener, H. Schwarz, P. W. Ingham and M. Hammerschmidt (2010). "Genetic analysis of fin development in zebrafish identifies furin and hemicentin1 as potential novel fraser syndrome disease genes." PLoS Genet **6**(4): e1000907.

Castro-Sanchez, L., A. Soto-Guzman, N. Navarro-Tito, R. Martinez-Orozco and E. P. Salazar (2010). "Native type IV collagen induces cell migration through a CD9 and DDR1-dependent pathway in MDA-MB-231 breast cancer cells." Eur J Cell Biol **89**(11): 843-852.

Ceron, J., J. F. Rual, A. Chandra, D. Dupuy, M. Vidal and S. van den Heuvel (2007). "Large-scale RNAi screens identify novel genes that interact with the C. elegans retinoblastoma pathway as well as splicing-related components with synMuv B activity." BMC Dev Biol **7**: 30.

Chapman, J. O., H. Li and E. A. Lundquist (2008). "The MIG-15 NIK kinase acts cell-autonomously in neuroblast polarization and migration in C. elegans." Dev Biol **324**(2): 245-257.

Chastney, M. R., J. R. W. Conway and J. Ivaska (2021). "Integrin adhesion complexes." Curr Biol **31**(10): R536-R542.

Chen, L., X. Kong, Y. Fang, S. Paunikar, X. Wang, J. A. L. Brown, E. Bourke, X. Li and J. Wang (2021). "Recent Advances in the Role of Discoidin Domain Receptor Tyrosine Kinase 1 and Discoidin Domain Receptor Tyrosine Kinase 2 in Breast and Ovarian Cancer." Front Cell Dev Biol **9**: 747314.

Clay, M. R. and D. R. Sherwood (2015). "Basement Membranes in the Worm: A Dynamic Scaffolding that Instructs Cellular Behaviors and Shapes Tissues." Curr Top Membr **76**: 337-371.

Conklin, M. W., A. Ada-Nguema, M. Parsons, K. M. Riching and P. J. Keely (2010). "R-Ras regulates beta1-integrin trafficking via effects on membrane ruffling and endocytosis." BMC Cell Biol **11**: 14.

881 Corcoran, D. S., V. Juskaite, Y. Xu, F. Gorlitz, Y. Alexandrov, C. Dunsby, P. M. W. French and
882 B. Leitinger (2019). "DDR1 autophosphorylation is a result of aggregation into dense clusters."
883 Sci Rep **9**(1): 17104.
884 Dickinson, D. J., J. D. Ward, D. J. Reiner and B. Goldstein (2013). "Engineering the
885 Caenorhabditis elegans genome using Cas9-triggered homologous recombination." Nat
886 Methods **10**(10): 1028-1034.
887 Edelstein, A., N. Amodaj, K. Hoover, R. Vale and N. Stuurman (2010). "Computer control of
888 microscopes using microManager." Curr Protoc Mol Biol **Chapter 14**: Unit14 20.
889 Feitosa, N. M., J. Zhang, T. J. Carney, M. Metzger, V. Korzh, W. Bloch and M. Hammerschmidt
890 (2012). "Hemicentin 2 and Fibulin 1 are required for epidermal-dermal junction formation and fin
891 mesenchymal cell migration during zebrafish development." Dev Biol **369**(2): 235-248.
892 Fidler, A. L., S. P. Boudko, A. Rokas and B. G. Hudson (2018). "The triple helix of collagens - an
893 ancient protein structure that enabled animal multicellularity and tissue evolution." J Cell Sci
894 **131**(7).
895 Frische, E. W., W. Pellis-van Berkel, G. van Haaften, E. Cuppen, R. H. Plasterk, M. Tijsterman,
896 J. L. Bos and F. J. Zwartkruis (2007). "RAP-1 and the RAL-1/exocyst pathway coordinate
897 hypodermal cell organization in Caenorhabditis elegans." EMBO J **26**(24): 5083-5092.
898 Frokjaer-Jensen, C., M. W. Davis, M. Ailion and E. M. Jorgensen (2012). "Improved Mos1-
899 mediated transgenesis in C. elegans." Nat Methods **9**(2): 117-118.
900 Fu, H. L., R. R. Valiathan, R. Arkwright, A. Sohail, C. Mihai, M. Kumarasiri, K. V. Mahasenan, S.
901 Mobashery, P. Huang, G. Agarwal and R. Fridman (2013). "Discoidin domain receptors: unique
902 receptor tyrosine kinases in collagen-mediated signaling." J Biol Chem **288**(11): 7430-7437.
903 Gao, Y., D. Mruk, H. Chen, W. Y. Lui, W. M. Lee and C. Y. Cheng (2017). "Regulation of the
904 blood-testis barrier by a local axis in the testis: role of laminin alpha2 in the basement
905 membrane." FASEB J **31**(2): 584-597.
906 Ghosh, S. and P. W. Sternberg (2014). "Spatial and molecular cues for cell outgrowth during C.
907 elegans uterine development." Dev Biol **396**(1): 121-135.
908 Gianakas, C. A., D. P. Keeley, W. Ramos-Lewis, K. Park, R. Jayadev, I. W. Kenny, Q. Chi and
909 D. R. Sherwood (2023). "Hemicentin-mediated type IV collagen assembly strengthens
910 juxtaposed basement membrane linkage." J Cell Biol **222**(1).
911 Gieseler, K., H. Qadota and G. M. Benian (2017). "Development, structure, and maintenance of
912 C. elegans body wall muscle." WormBook **2017**: 1-59.
913 Goh, L. K. and A. Sorkin (2013). "Endocytosis of receptor tyrosine kinases." Cold Spring Harb
914 Perspect Biol **5**(5): a017459.
915 Gross, O., B. Beirowski, S. J. Harvey, C. McFadden, D. Chen, S. Tam, P. S. Thorner, N. Smyth,
916 K. Addicks, W. Bloch, Y. Ninomiya, Y. Sado, M. Weber and W. F. Vogel (2004). "DDR1-deficient
917 mice show localized subepithelial GBM thickening with focal loss of slit diaphragms and
918 proteinuria." Kidney Int **66**(1): 102-111.
919 Hagedorn, E. J., H. Yashiro, J. W. Ziel, S. Ihara, Z. Wang and D. R. Sherwood (2009). "Integrin
920 acts upstream of netrin signaling to regulate formation of the anchor cell's invasive membrane in
921 C. elegans." Dev Cell **17**(2): 187-198.
922 Hisamoto, N., Y. Nagamori, T. Shimizu, S. I. Pastuhov and K. Matsumoto (2016). "The C.
923 elegans Discoidin Domain Receptor DDR-2 Modulates the Met-like RTK-JNK Signaling
924 Pathway in Axon Regeneration." PLoS Genet **12**(12): e1006475.
925 Hohenester, E. and P. D. Yurchenco (2013). "Laminins in basement membrane assembly." Cell
926 Adh Migr **7**(1): 56-63.
927 Jayadev, R., Q. Chi, D. P. Keeley, E. L. Hastie, L. C. Kelley and D. R. Sherwood (2019). "alpha-
928 Integrins dictate distinct modes of type IV collagen recruitment to basement membranes." J Cell
929 Biol **218**(9): 3098-3116.
930 Jayadev, R., M. Morais, J. M. Ellingford, S. Srinivasan, R. W. Naylor, C. Lawless, A. S. Li, J. F.
931 Ingham, E. Hastie, Q. Chi, M. Fresquet, N. M. Koudis, H. B. Thomas, R. T. O'Keefe, E. Williams,

932 A. Adamson, H. M. Stuart, S. Banka, D. Smedley, C. Genomics England Research, D. R.
933 Sherwood and R. Lennon (2022). "A basement membrane discovery pipeline uncovers network
934 complexity, regulators, and human disease associations." Sci Adv **8**(20): eabn2265.
935 Jayadev, R. and D. R. Sherwood (2017). "Basement membranes." Curr Biol **27**(6): R207-R211.
936 Juskaite, V., D. S. Corcoran and B. Leitinger (2017). "Collagen induces activation of DDR1
937 through lateral dimer association and phosphorylation between dimers." Elife **6**.
938 Kamath, R. S. and J. Ahringer (2003). "Genome-wide RNAi screening in Caenorhabditis
939 elegans." Methods **30**(4): 313-321.
940 Keeley, D. P., E. Hastie, R. Jayadev, L. C. Kelley, Q. Chi, S. G. Payne, J. L. Jeger, B. D.
941 Hoffman and D. R. Sherwood (2020). "Comprehensive Endogenous Tagging of Basement
942 Membrane Components Reveals Dynamic Movement within the Matrix Scaffolding." Dev Cell
943 **54**(1): 60-74 e67.
944 Keeley, D. P. and D. R. Sherwood (2019). "Tissue linkage through adjoining basement
945 membranes: The long and the short term of it." Matrix Biol **75-76**: 58-71.
946 Kelley, L. C., Q. Chi, R. Caceres, E. Hastie, A. J. Schindler, Y. Jiang, D. Q. Matus, J. Plastino
947 and D. R. Sherwood (2019). "Adaptive F-Actin Polymerization and Localized ATP Production
948 Drive Basement Membrane Invasion in the Absence of MMPs." Dev Cell **48**(3): 313-328 e318.
949 Kelley, L. C., Z. Wang, E. J. Hagedorn, L. Wang, W. Shen, S. Lei, S. A. Johnson and D. R.
950 Sherwood (2017). "Live-cell confocal microscopy and quantitative 4D image analysis of anchor-
951 cell invasion through the basement membrane in Caenorhabditis elegans." Nat Protoc **12**(10):
952 2081-2096.
953 Khoshnoodi, J., V. Pedchenko and B. G. Hudson (2008). "Mammalian collagen IV." Microsc Res
954 Tech **71**(5): 357-370.
955 Lee, M., E. J. Cram, B. Shen and J. E. Schwarzbauer (2001). "Roles for beta(pat-3) integrins in
956 development and function of Caenorhabditis elegans muscles and gonads." J Biol Chem
957 **276**(39): 36404-36410.
958 Leitinger, B. (2014). "Discoidin domain receptor functions in physiological and pathological
959 conditions." Int Rev Cell Mol Biol **310**: 39-87.
960 Lilja, J., T. Zacharchenko, M. Georgiadou, G. Jacquemet, N. De Franceschi, E. Peuhu, H.
961 Hamidi, J. Pouwels, V. Martens, F. H. Nia, M. Beifuss, T. Boeckers, H. J. Kreienkamp, I. L.
962 Barsukov and J. Ivaska (2017). "SHANK proteins limit integrin activation by directly interacting
963 with Rap1 and R-Ras." Nat Cell Biol **19**(4): 292-305.
964 Martin-Bermudo, M. D. and N. H. Brown (1999). "Uncoupling integrin adhesion and signaling:
965 the betaPS cytoplasmic domain is sufficient to regulate gene expression in the Drosophila
966 embryo." Genes Dev **13**(6): 729-739.
967 Merchant, S. N., B. J. Burgess, J. C. Adams, C. E. Kashtan, M. C. Gregory, P. A. Santi, R.
968 Colvin, B. Collins and J. B. Nadol, Jr. (2004). "Temporal bone histopathology in alport
969 syndrome." Laryngoscope **114**(9): 1609-1618.
970 Mihai, C., M. Chotani, T. S. Elton and G. Agarwal (2009). "Mapping of DDR1 distribution and
971 oligomerization on the cell surface by FRET microscopy." J Mol Biol **385**(2): 432-445.
972 Moerman, D. G. and B. D. Williams (2006). "Sarcomere assembly in C. elegans muscle."
973 WormBook: 1-16.
974 Mok, D. Z., P. W. Sternberg and T. Inoue (2015). "Morphologically defined sub-stages of C.
975 elegans vulval development in the fourth larval stage." BMC Dev Biol **15**: 26.
976 Morrissey, M. A., D. P. Keeley, E. J. Hagedorn, S. T. H. McClatchey, Q. Chi, D. H. Hall and D.
977 R. Sherwood (2014). "B-LINK: a hemicentin, plakin, and integrin-dependent adhesion system
978 that links tissues by connecting adjacent basement membranes." Dev Cell **31**(3): 319-331.
979 Morrissey, M. A. and D. R. Sherwood (2015). "An active role for basement membrane assembly
980 and modification in tissue sculpting." J Cell Sci **128**(9): 1661-1668.
981 Murphy, J. E., B. E. Padilla, B. Hasdemir, G. S. Cottrell and N. W. Bunnett (2009). "Endosomes:
982 a legitimate platform for the signaling train." Proc Natl Acad Sci U S A **106**(42): 17615-17622.

983 Naylor, R. W., M. Morais and R. Lennon (2021). "Complexities of the glomerular basement
984 membrane." Nat Rev Nephrol **17**(2): 112-127.
985 Newman, A. P., J. G. White and P. W. Sternberg (1996). "Morphogenesis of the C. elegans
986 hermaphrodite uterus." Development **122**(11): 3617-3626.
987 Pani, A. M. and B. Goldstein (2018). "Direct visualization of a native Wnt in vivo reveals that a
988 long-range Wnt gradient forms by extracellular dispersal." Elife **7**.
989 Park, J. O., J. Pan, F. Mohrlen, M. O. Schupp, R. Johnsen, D. L. Baillie, R. Zapf, D. G.
990 Moerman and H. Hutter (2010). "Characterization of the astacin family of metalloproteases in C.
991 elegans." BMC Dev Biol **10**: 14.
992 Payne, L. S. and P. H. Huang (2014). "Discoidin domain receptor 2 signaling networks and
993 therapy in lung cancer." J Thorac Oncol **9**(6): 900-904.
994 Pozzi, A., P. D. Yurchenco and R. V. Iozzo (2017). "The nature and biology of basement
995 membranes." Matrix Biol **57-58**: 1-11.
996 Rual, J. F., J. Ceron, J. Koreth, T. Hao, A. S. Nicot, T. Hirozane-Kishikawa, J. Vandenhaute, S.
997 H. Orkin, D. E. Hill, S. van den Heuvel and M. Vidal (2004). "Toward improving Caenorhabditis
998 elegans phenome mapping with an ORFeome-based RNAi library." Genome Res **14**(10B):
999 2162-2168.
1000 Sandri, C., F. Caccavari, D. Valdembri, C. Camillo, S. Veltel, M. Santambrogio, L. Lanzetti, F.
1001 Bussolino, J. Ivaska and G. Serini (2012). "The R-Ras/RIN2/Rab5 complex controls endothelial
1002 cell adhesion and morphogenesis via active integrin endocytosis and Rac signaling." Cell Res
1003 **22**(10): 1479-1501.
1004 Sato, K., A. Norris, M. Sato and B. D. Grant (2014). "C. elegans as a model for membrane
1005 traffic." WormBook: 1-47.
1006 Schindelin, J., I. Arganda-Carreras, E. Frise, V. Kaynig, M. Longair, T. Pietzsch, S. Preibisch, C.
1007 Rueden, S. Saalfeld, B. Schmid, J. Y. Tinevez, D. J. White, V. Hartenstein, K. Eliceiri, P.
1008 Tomancak and A. Cardona (2012). "Fiji: an open-source platform for biological-image analysis."
1009 Nat Methods **9**(7): 676-682.
1010 Sherwood, D. R. and P. W. Sternberg (2003). "Anchor cell invasion into the vulval epithelium in
1011 C. elegans." Dev Cell **5**(1): 21-31.
1012 Singh, N. and M. Han (1995). "sur-2, a novel gene, functions late in the let-60 ras-mediated
1013 signaling pathway during Caenorhabditis elegans vulval induction." Genes Dev **9**(18): 2251-
1014 2265.
1015 Sixt, M., B. Engelhardt, F. Pausch, R. Hallmann, O. Wendler and L. M. Sorokin (2001).
1016 "Endothelial cell laminin isoforms, laminins 8 and 10, play decisive roles in T cell recruitment
1017 across the blood-brain barrier in experimental autoimmune encephalomyelitis." J Cell Biol
1018 **153**(5): 933-946.
1019 Staudinger, L. A., S. J. Spano, W. Lee, N. Coelho, D. Rajshankar, M. P. Bendeck, T. Moriarty
1020 and C. A. McCulloch (2013). "Interactions between the discoidin domain receptor 1 and beta1
1021 integrin regulate attachment to collagen." Biol Open **2**(11): 1148-1159.
1022 Stiernagle, T. (2006). "Maintenance of C. elegans." WormBook: 1-11.
1023 Suleiman, H., L. Zhang, R. Roth, J. E. Heuser, J. H. Miner, A. S. Shaw and A. Dani (2013).
1024 "Nanoscale protein architecture of the kidney glomerular basement membrane." Elife **2**: e01149.
1025 Taylor, J., T. Unsoeld and H. Hutter (2018). "The transmembrane collagen COL-99 guides
1026 longitudinally extending axons in C. elegans." Mol Cell Neurosci **89**: 9-19.
1027 Timmons, L., D. L. Court and A. Fire (2001). "Ingestion of bacterially expressed dsRNAs can
1028 produce specific and potent genetic interference in Caenorhabditis elegans." Gene **263**(1-2):
1029 103-112.
1030 Tu, H., P. Huhtala, H. M. Lee, J. C. Adams and T. Pihlajaniemi (2015). "Membrane-associated
1031 collagens with interrupted triple-helices (MACITs): evolution from a bilaterian common ancestor
1032 and functional conservation in C. elegans." BMC Evol Biol **15**: 281.

1033 Unsoeld, T., J. O. Park and H. Hutter (2013). "Discoidin domain receptors guide axons along
1034 longitudinal tracts in C. elegans." Dev Biol **374**(1): 142-152.
1035 Villasenor, R., Y. Kalaidzidis and M. Zerial (2016). "Signal processing by the endosomal
1036 system." Curr Opin Cell Biol **39**: 53-60.
1037 Vogel, B. E. and E. M. Hedgecock (2001). "Hemicentin, a conserved extracellular member of
1038 the immunoglobulin superfamily, organizes epithelial and other cell attachments into oriented
1039 line-shaped junctions." Development **128**(6): 883-894.
1040 Vogel, W. F., R. Abdulhussein and C. E. Ford (2006). "Sensing extracellular matrix: an update
1041 on discoidin domain receptor function." Cell Signal **18**(8): 1108-1116.
1042 Walser, M., C. A. Umbricht, E. Frohli, P. Nanni and A. Hajnal (2017). "beta-Integrin de-
1043 phosphorylation by the Density-Enhanced Phosphatase DEP-1 attenuates EGFR signaling in C.
1044 elegans." PLoS Genet **13**(1): e1006592.
1045 Welcker, D., C. Stein, N. M. Feitosa, J. Armistead, J. L. Zhang, S. Lutke, A. Kleinridders, J. C.
1046 Bruning, S. A. Eming, G. Sengle, A. Niehoff, W. Bloch and M. Hammerschmidt (2021).
1047 "Hemicentin-1 is an essential extracellular matrix component of the dermal-epidermal and
1048 myotendinous junctions." Sci Rep **11**(1): 17926.
1049 Wildwater, M., N. Sander, G. de Vreede and S. van den Heuvel (2011). "Cell shape and Wnt
1050 signaling redundantly control the division axis of C. elegans epithelial stem cells." Development
1051 **138**(20): 4375-4385.
1052 Xiao, Q., Y. Jiang, Q. Liu, J. Yue, C. Liu, X. Zhao, Y. Qiao, H. Ji, J. Chen and G. Ge (2015).
1053 "Minor Type IV Collagen alpha5 Chain Promotes Cancer Progression through Discoidin Domain
1054 Receptor-1." PLoS Genet **11**(5): e1005249.
1055 Xu, H., D. Bihan, F. Chang, P. H. Huang, R. W. Farndale and B. Leitinger (2012). "Discoidin
1056 domain receptors promote alpha1beta1- and alpha2beta1-integrin mediated cell adhesion to
1057 collagen by enhancing integrin activation." PLoS One **7**(12): e52209.
1058 Yochem, J. and R. K. Herman (2003). "Investigating C. elegans development through mosaic
1059 analysis." Development **130**(20): 4761-4768.
1060 Zhang, Z., K. Vuori, H. Wang, J. C. Reed and E. Ruoslahti (1996). "Integrin activation by R-ras."
1061 Cell **85**(1): 61-69.
1062

## Figure 1

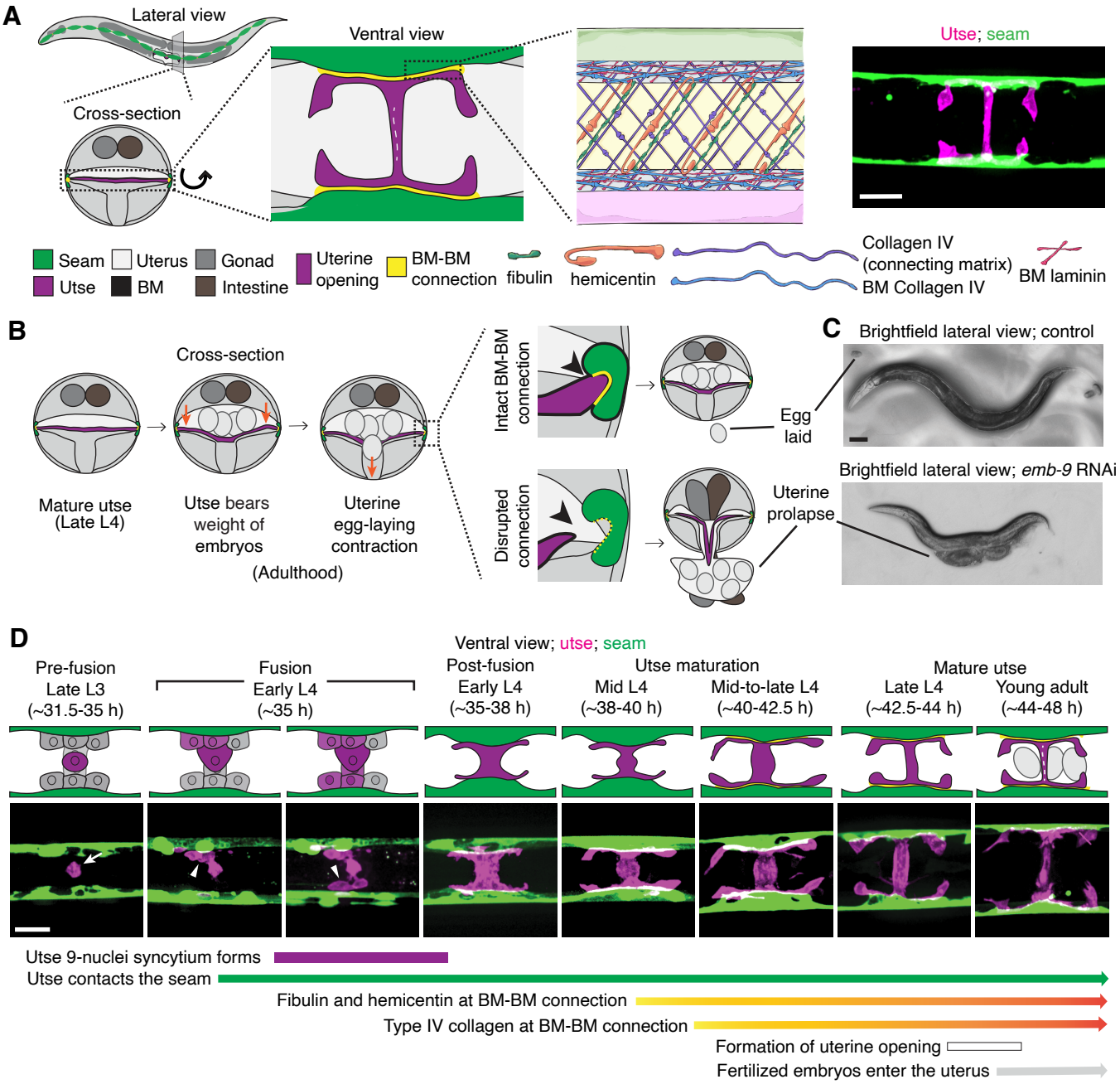


**Morphogenesis of the *C. elegans* utse-seam basement membrane-basement membrane tissue connection.**
(**A**) Left and center: Schematic depicting the utse-seam connection. The utse (a syncytial uterine cell) and the seam epidermal cells are both encased in basement membranes (BMs), which are linked by a BM-BM connecting matrix. Right: ventral fluorescence z-projection showing the utse and seam cells visualized by the markers *cdh-3p::mCherry::PLC* $^{\delta PH}$ and *scmp::GFP::CAAX*, respectively. (**B**) Schematic illustrating the role of the utse-seam connection in supporting the uterus during egg-laying muscle contractions. Disruption of the connection results in uterine prolapse. (**C**) Lateral brightfield images of adult worms on control RNAi treatment or RNAi against a key component of the BM-BM linkage, $\alpha$1 type IV collagen/*emb-9* (RNAi fed from the L1 onward); note the uterine prolapse after loss of collagen. (**D**) A schematic summarizing the development of the utse-seam connection. Fluorescence images shown are ventral z-projections of the utse and the seam at the respective developmental stages from the late L3 to young adult (hours post-hatch at 20°C). Arrow indicates the uterine anchor cell (AC) that fuses with adjacent uterine cells to form the utse. During syncytium formation, the utse makes contact with the seam cells (arrowheads). Scale bars, 20 $\mu$m.

## **Figure 2** with 1 supplement

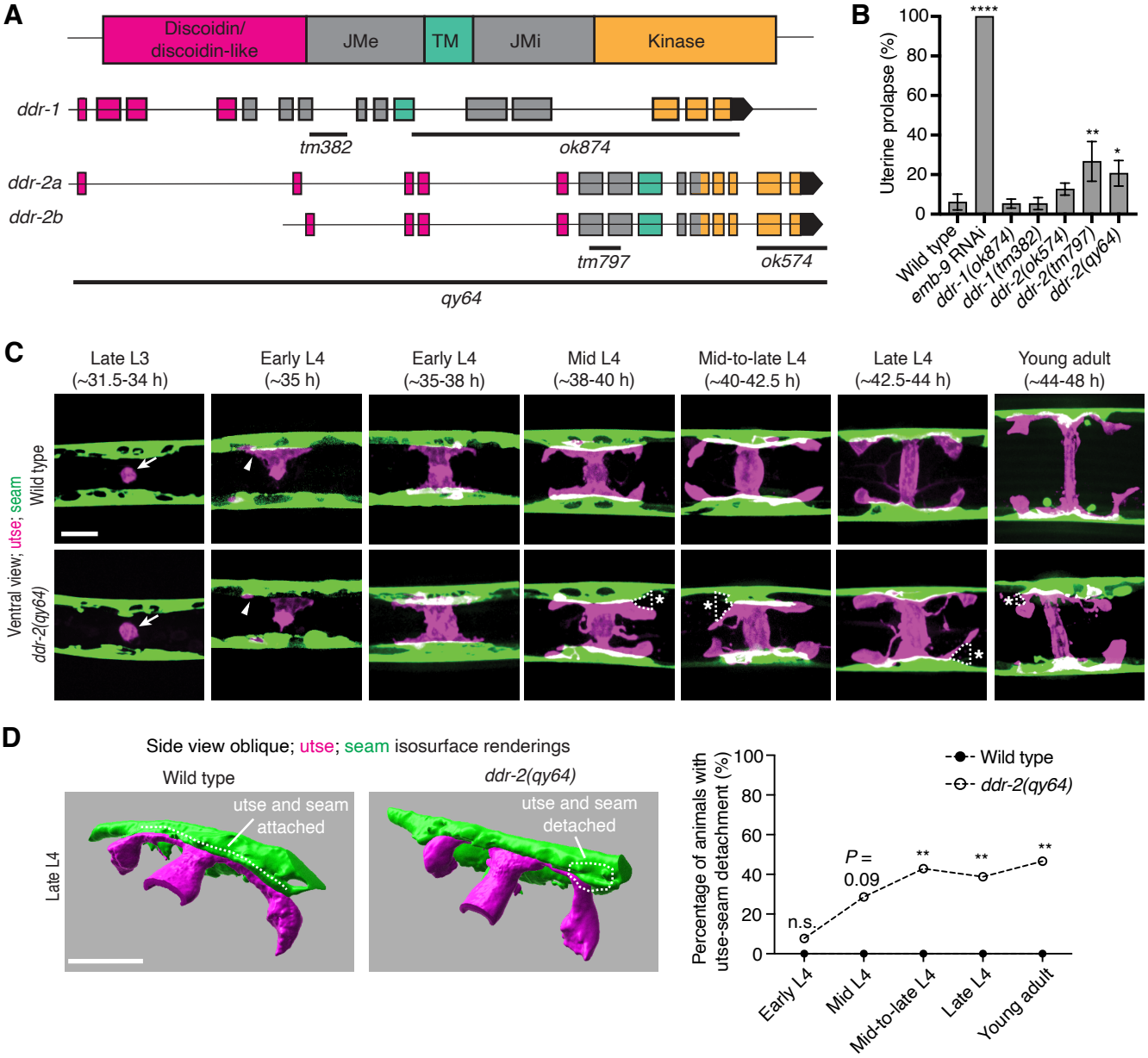


**DDR-2 promotes utse-seam attachment and protects against uterine prolapse.**
(**A**) Domain structure of *C. elegans* discoidin domain receptors (DDRs) and exon-intron gene structures of *ddr-1* and *ddr-2*. Exons are color coded according to respective domains. Gene regions that are deleted in respective mutant alleles (italicized text) are demarcated by solid black lines. (**B**) Frequency of uterine prolapse in *ddr-1* and *ddr-2* mutant animals compared to wild type. Data are shown as mean prolapse percentage ± SD, derived from three independent trials (n = 50 animals screened per trial). α1 type IV collagen/*emb-9* RNAi was used as a positive control. ****$P \leq 0.0001$, **$P \leq 0.01$, *$P \leq 0.05$; one-way ANOVA with post hoc Dunnett's test. (**C**) Ventral fluorescence z-projections of the utse *(cdh-3p::mCherry::PLC $^{\delta PH}$)* and seam *(scmp::GFP::CAAX)* cells in wild-type and *ddr-2* knockout *(ddr-2(qy64))* animals from the late L3 to young adult developmental stages. Arrows indicate the AC prior to utse formation and arrowheads denote early contacts between the utse and seam. Dotted lines with asterisks indicate regions of utse-seam detachment in *ddr-2(qy64)* animals. (**D**) Left: 3D isosurface renderings of the utse and seam in representative late L4 wild-type and *ddr-2(qy64)* animals (see also ***Figure 2—video 1***). Right: Quantification of the percentage of animals with utse-seam detachment. Wild type, early L4 to young adult: n = 0/13, n = 0/14, n = 0/22, n = 0/21, n = 0/18 animals with detachments respectively; *ddr-2(qy64)*, early L4 to young adult: n = 1/13, n = 4/14, n = 9/22, n = 7/18, n = 7/15 animals with detachments respectively. **$P \leq 0.01$, n.s. (not significant), $P > 0.05$; Fisher's exact test. Scale bars, 20 μm.

**Source data 1.** Source data for ***Figure 2***. Raw data of uterine prolapse frequency used to generate ***Figure 2B*** in Microsoft Excel format.

**Figure 2—video 1.** Animation of 3D isosurface rendering of the utse and seam in a representative late L4 wild-type animal; related to ***Figure 2D***.

## **Figure 3** with 1 supplement

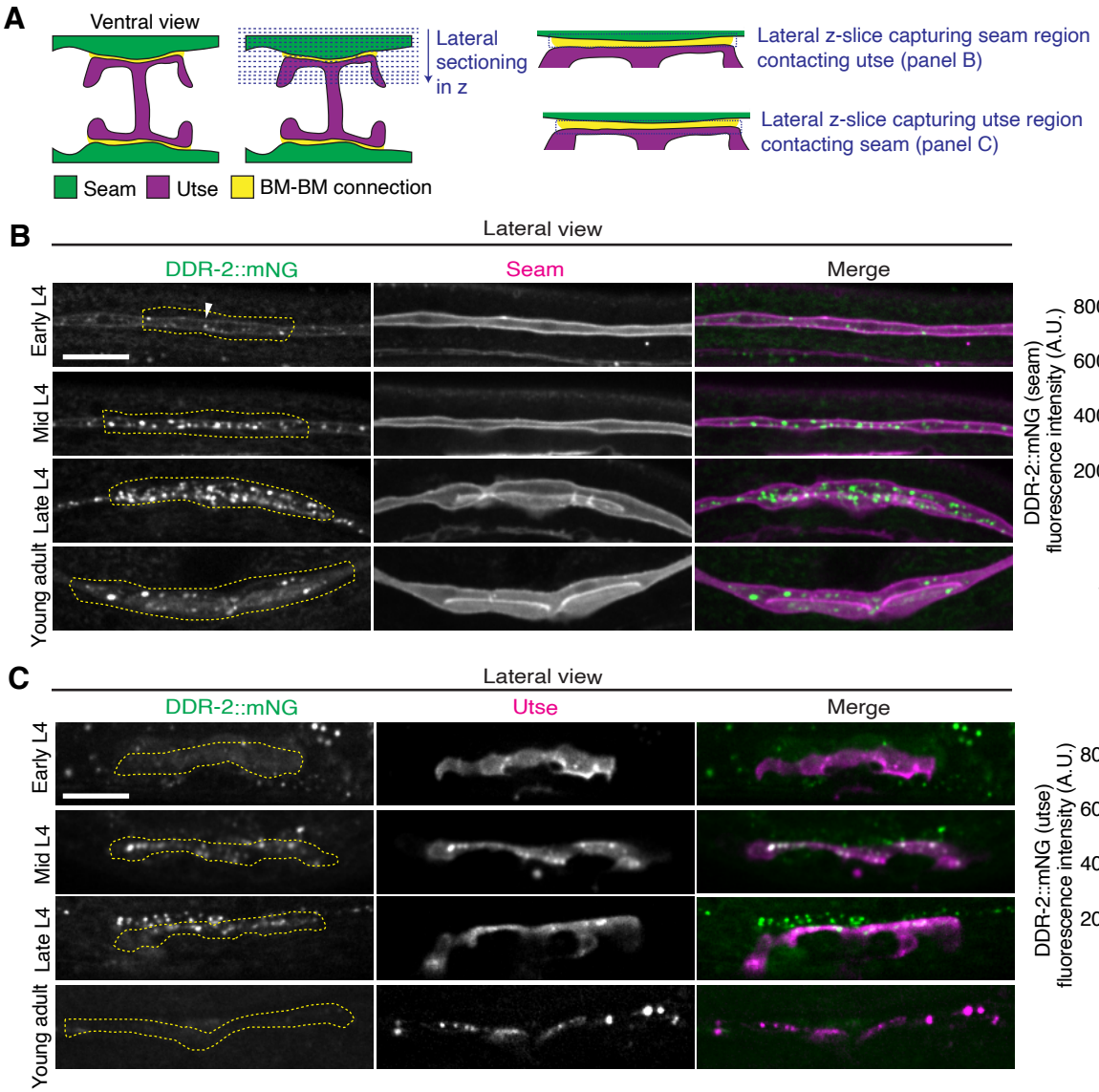


**DDR-2 levels peak in the utse and seam during the formation of the BM-BM connection.**
(**A**) Schematic illustrating lateral z-sectioning to determine slices that capture the seam region in contact with the utse and vice-versa. (**B**) Left: Lateral fluorescence images of DDR-2::mNG visualized with the seam marker *scmp::2xmKate2::PLC* $^{\delta PH}$ from the early L4 to young adult stages. Dotted yellow regions indicate DDR-2 signal in the seam contacting the utse. White arrowhead denotes DDR-2 signal at the cell surface. Right: Quantification of mean DDR-2::mNG fluorescence intensity in the dotted regions (n ≥ 9 for each developmental stage). ****$P \leq 0.0001$, one-way ANOVA with post hoc Dunnett's test. (**C**) Left: Lateral fluorescence images of DDR-2::mNG visualized with the utse marker *cdh-3p::mCherry::PLC* $^{\delta PH}$ from the early L4 to young adult stages. Dotted yellow regions indicate DDR-2 signal in the utse contacting the seam. Right: Quantification of mean DDR-2::mNG fluorescence intensity in dotted yellow regions (n = 10 all stages). **$P \leq 0.01$, one-way ANOVA with post hoc Dunnett's test. Scale bars, 20 $\mu$m. Box edges in boxplots represent the 25th and 75th percentiles, the line in the box denotes the median value, and whiskers mark the minimum and maximum values.

**Source data 1.** Source data for ***Figure 3***. Raw data of DDR-2::mNG fluorescence intensity quantification in the seam and utse used to generate boxplots in ***Figure 3B and C*** in Microsoft Excel format. Note that boxplot in ***Figure 3—figure supplement 1A*** was also generated from these data.
**Source data 2.** Source data for ***Figure 3—figure supplement 1***. Raw data of DDR-2::mNG and mCherry-tagged vesicle marker co-localization analysis used to generate boxplots in ***Figure 3—figure supplement 1B and C*** in Microsoft Excel format.

**Figure supplement 1.** DDR-2 is found within endocytic vesicles; related to ***Figure 3B and C***.

## Figure 3—figure supplement 1

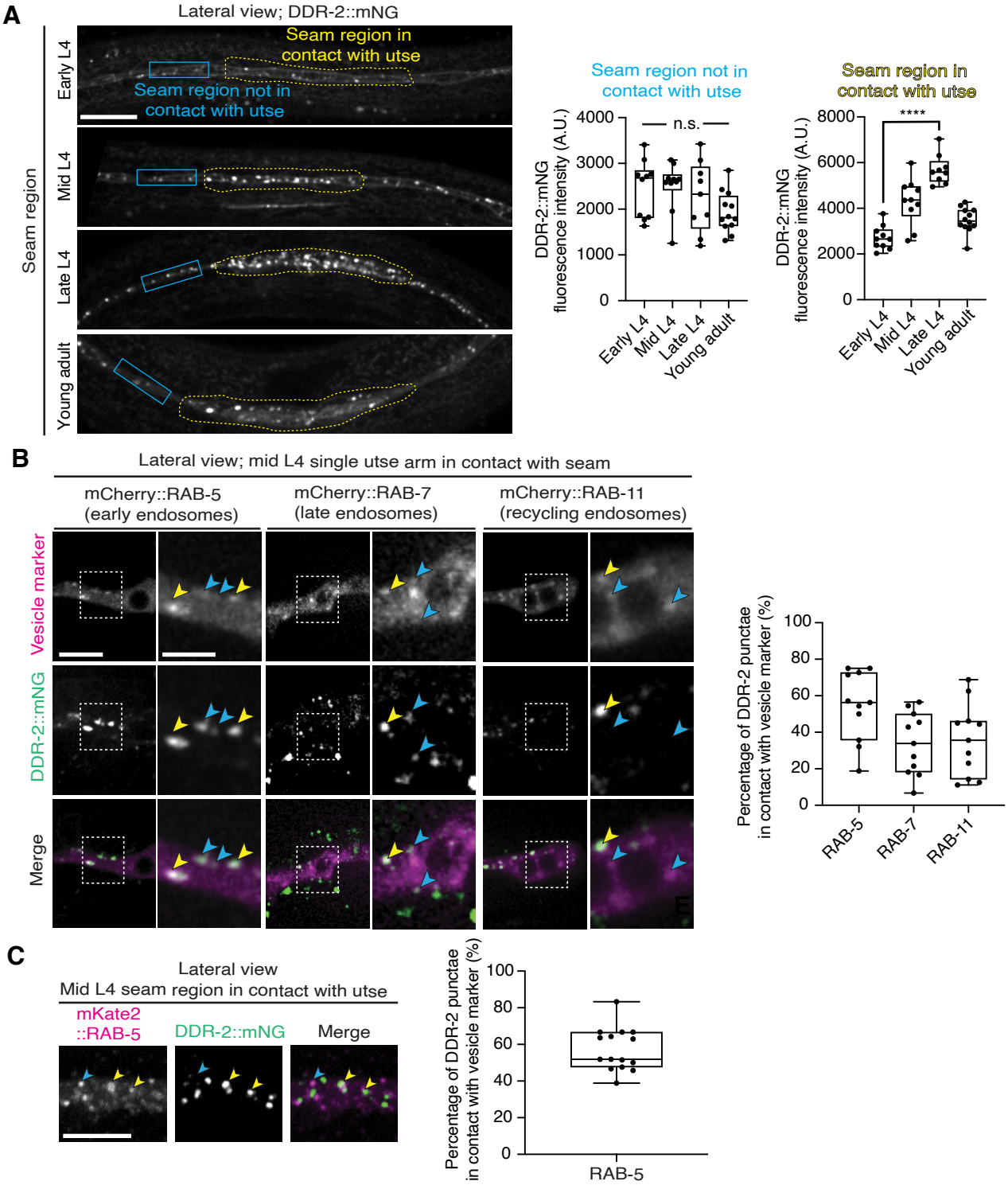


**DDR-2 is found within endocytic vesicles.**
Related to ***Figure 3***. (**A**) Lateral fluorescence images of DDR-2::mNG in the seam cells from the early L4 to young adult stages. Note that these images are the same animals as in ***Figure 3B*** with a larger cropped field of view to include regions of the seam not in contact with the utse. Quantification of mean fluorescence intensity in the blue and yellow boxed regions is shown on the right (n ≥ 9 all stages). Boxplots for yellow boxed regions are reproduced from ***Figure 3B***. n.s. (not significant), $P > 0.05$; Kruskal-Wallis $H$ test. ****$P \leq 0.0001$, one-way ANOVA with post hoc Dunnett's test. (**B**) Lateral fluorescence images of DDR-2::mNG within a single arm of the utse tissue at the mid L4 stage, visualized together with mCherry-tagged RAB-5, RAB-7, or RAB-11. Boxed regions are magnified on the right. Yellow arrowheads denote DDR-2 punctae in contact with the respective vesicle marker, while blue arrowheads correspond to DDR-2 puncta that not in contact with vesicle markers. The boxplot shows quantification of percentage overlap of DDR-2 punctae with vesicle markers (n = 11 animals per marker). (**C**) Left: Lateral fluorescence images of DDR-2::mNG and mKate2::RAB-5 in the seam region contacting the utse. Arrowheads denote DDR-2 punctae in contact with (yellow) or not in contact with (blue) mCherry::RAB-5 punctae. Right: Percentage overlap of DDR-2 punctae with RAB-5 (n = 15). Scale bars, 20 $\mu$m. Box edges in boxplots represent the 25th and 75th percentiles, the line in the box denotes the median value, and whiskers mark the minimum and maximum values.

## **Figure 4** with 1 supplement

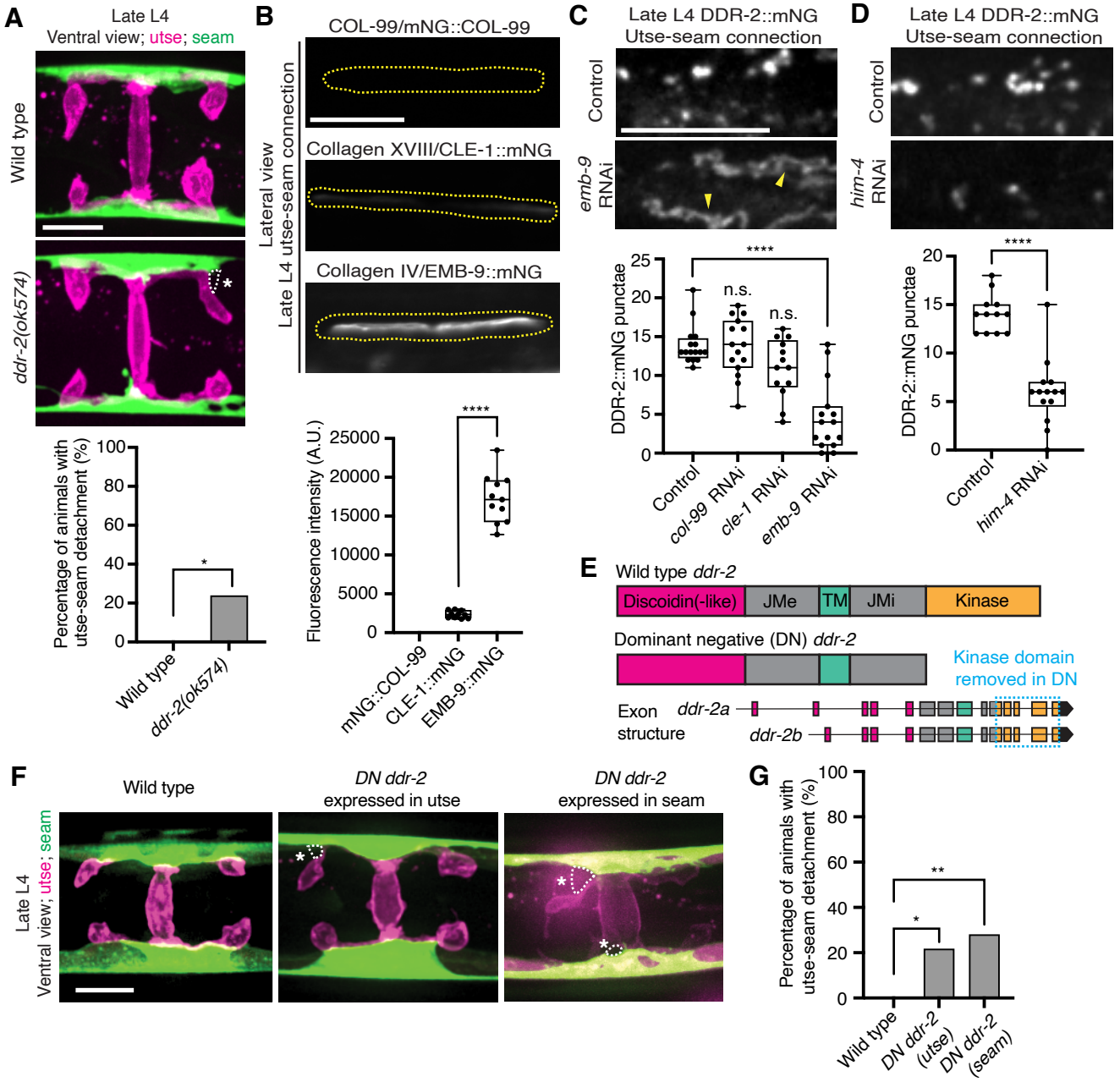


**DDR-2 endocytosis is triggered by type IV collagen and DDR-2 is required in both the utse and seam to promote tissue connection.**
(**A**) Top: Ventral fluorescence z-projections of the utse *(nas-22p::2xmKate2::PLC* $^{\delta PH}$*)* and seam *(scmp::GFP::CAAX)* cells in late L4 wild-type and *ddr-2* kinase domain truncation mutant *(ddr-2(ok574))* animals. Dotted lines with asterisks indicate regions of utse-seam detachment. Bottom: Quantification of the percentage of animals with utse-seam detachment. Wild type, n = 0/26; *ddr-2(ok574)*, n = 5/21 animals with detachments respectively. $^{**}P \leq 0.01$, Fisher's exact test. (**B**) Top: Lateral fluorescence images of COL-99 (mNG::COL-99), type XVIII collagen (CLE-1::mNG), and α1 type IV collagen (EMB-9::mNG) at the utse-seam connection (dotted yellow regions) of late L4 animals. All images were acquired at the same exposure. Bottom: Quantification of mean fluorescence intensity (n ≥ 10 for each fluorescent protein). $^{****}P \leq 0.0001$, unpaired two-tailed Student's *t* test. (**C**) Top: Lateral fluorescence z-projections of DDR-2::mNG at the utse-seam connection in control or *emb-9* RNAi-treated late L4 animals. Note that the field of view contains a single utse arm contacting the seam tissue. Arrowheads indicate cell surface accumulation of DDR-2 upon collagen IV depletion. Bottom: Quantification of the average number of discrete DDR-2 punctae at the utse-seam connection on control, *col-99*, *cle-1*, or *emb-9* RNAi treatments (n ≥ 13 animals for all treatments). $^{****}P \leq 0.0001$, n.s. (not significant), $P > 0.05$; Kruskal-Wallis *H* test with post hoc Dunn's test. (**D**) Top: Lateral fluorescence z-projections of DDR-2::mNG at the utse-seam attachment in control or hemicentin/*him-4* RNAi-treated late L4 animals. Bottom: Quantification of the average number of discrete DDR-2 punctae at the utse-seam attachment on control or *him-4* RNAi-treated animals (n ≥ 13 all treatments). $^{****}P \leq 0.0001$, Mann-Whitney *U* test. (**E**) Schematic of dominant negative (DN) *ddr-2*. (**F**) Ventral fluorescence z-projections of the utse *(nas-22p::2xmKate2::PLC* $^{\delta PH}$*)* and seam *(wrt-2p::GFP::PLC* $^{\delta PH}$*)* tissues in late L4 stage wild-type animals and animals expressing *DN ddr-2* in the utse (driven by *cdh-3* promoter) or the seam (driven by *scm* promoter). Dotted lines with asterisks indicate regions of utse-seam detachment. (**G**) Quantification of the percentage of animals with utse-seam detachment. Wild type, n = 0/23; *DN ddr-2(utse)*, n = 5/23; *DN ddr-2(seam)*, n = 7/25 animals with detachments respectively. $^{**}P \leq 0.01$ 0.01, $^{*}P \leq 0.05$; Fisher's exact test. Scale bars, 20 μm. Box edges in boxplots represent the 25th and 75th percentiles, the line in the box denotes the median value, and whiskers mark the minimum and maximum values.

**Source data 1.** Source data for ***Figure 4***. Raw data of fluorescence intensity quantification of tagged collagen ligands at the utse-seam connection used to generate boxplot in ***Figure 4B***, and raw data of DDR-2::mNG puncta counts at the utse-seam connection upon collagen ligand or hemicentin depletion used to generate boxplots in ***Figure 4C and D*** in Microsoft Excel format.
**Source data 2.** Source data for ***Figure 4—figure supplement 1***. Raw data of quantification of knockdown efficiencies of tagged collagen ligands and hemicentin at the utse-seam connection used to generate boxplots in ***Figure 4—figure supplement 1*** in Microsoft Excel format.

**Figure supplement 1.** Collagen and hemicentin knockdown efficiencies; related to ***Figure 4C and D***.

## Figure 4—figure supplement 1

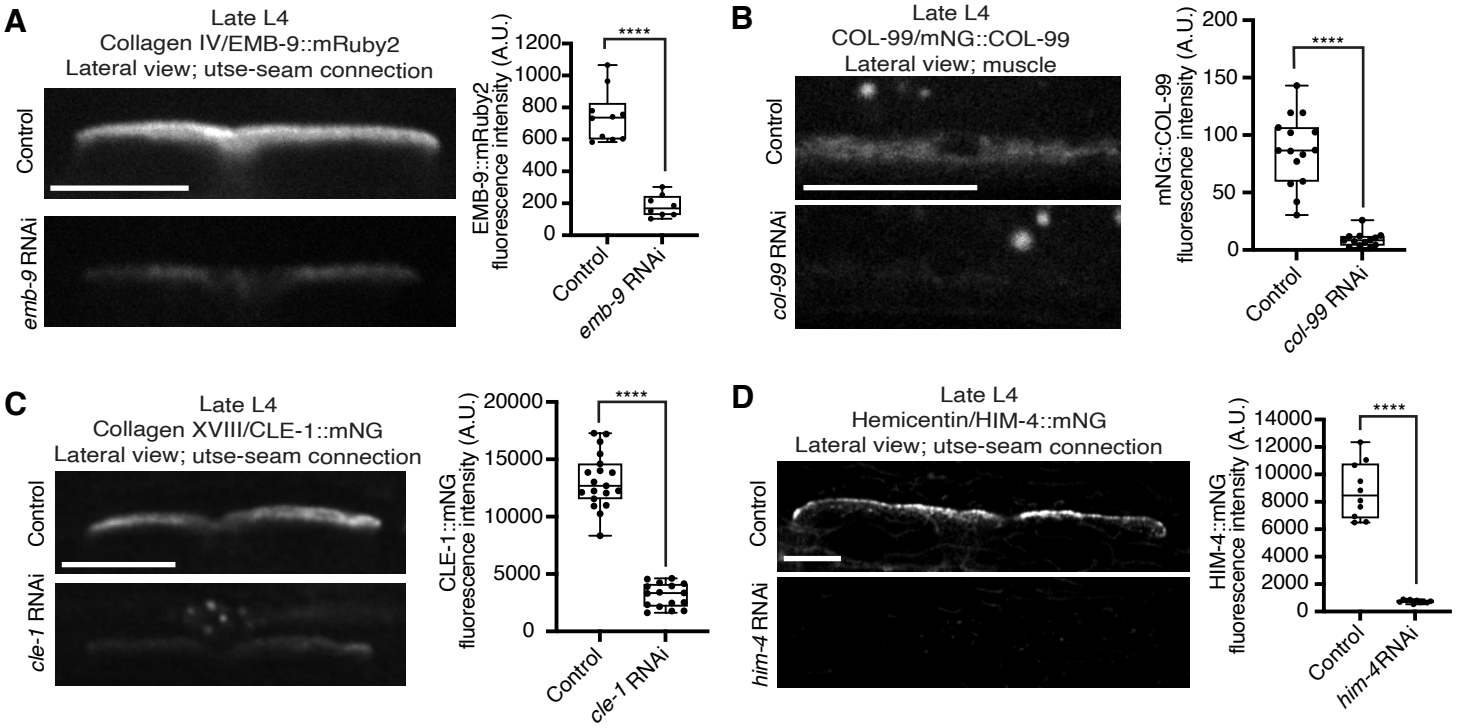


**Collagen and hemicentin knockdown efficiencies.**

Related to ***Figure 4***. (**A**) Lateral fluorescence images of EMB-9::mRuby2 (type IV collagen) at the utse-seam BM-BM connection in late L4 control or *emb-9* RNAi-treated animals. Mean fluorescence intensity quantified on the right (n ≥ 8 all treatments). (**B**) Lateral fluorescence images of mNG::COL-99 (COL-99) in the body wall muscle tissue in late L4 control or *col-99* RNAi-treated animals. Mean fluorescence intensity quantified on the right (n ≥ 13 all treatments). COL-99 signal in the muscle was analyzed as COL-99 was not detected at the utse-seam connection. (**C**) Lateral fluorescence images of CLE-1::mNG (type XVIII collagen) at the utse-seam BM-BM attachment in late L4 control or *cle-1* RNAi-treated animals. Mean fluorescence intensity quantified on the right (n ≥ 16 all treatments). (**D**) Lateral fluorescence images of HIM-4::mNG (hemicentin) at the utse-seam BM-BM connection in late L4 control or *him-4* RNAi-treated animals. Mean fluorescence intensity quantified on the right (n = 10 all treatments). ****$P \leq 0.0001$, unpaired two-tailed Student's *t* test (EMB-9, CLE-1, and HIM-4) or Mann-Whitney *U* test (COL-99). Scale bars, 20 $\mu$m. Box edges in boxplots represent the 25th and 75th percentiles, the line in the box denotes the median value, and whiskers mark the minimum and maximum values.

## **Figure 5** with 2 supplements

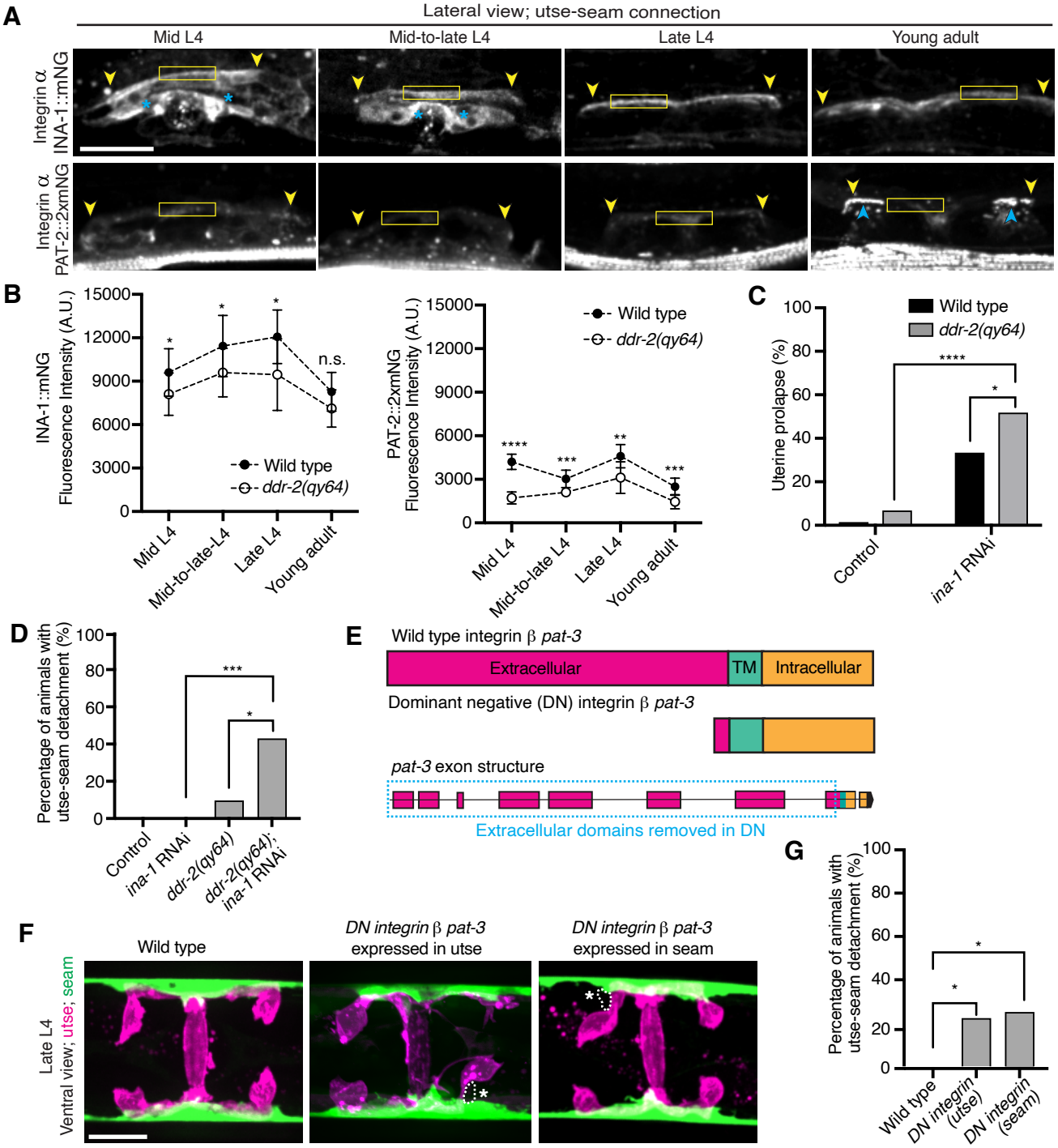


**DDR-2 regulates integrin levels at the utse-seam connection and integrin functions in the utse and seam to mediate tissue attachment.** (**A**) Lateral fluorescence z-projections of integrin α subunits INA-1::mNG and PAT-2::2XmNG at the utse-seam connection (yellow arrowheads) from the mid L4 to young adult stages. Blue asterisks and arrowheads denote INA-1 signal in the developing vulva and PAT-2 at muscle attachment sites respectively. Fluorescence intensity at the utse-seam connection measured in yellow boxes. (**B**) Quantification of mean fluorescence intensity in wild-type and *ddr-2* knockout *(ddr-2(qy64))* animals (n ≥ 9 all conditions). Error bars represent SD. ****$P \leq 0.0001$, ***$P \leq 0.001$, **$P \leq 0.01$, *$P \leq 0.05$, n.s. (not significant), $P > 0.05$; unpaired two-tailed Student's *t* test. (**C**) Frequency of uterine prolapse in wild-type and *ddr-2(qy64)* animals treated with control or *ina-1* RNAi. Control n = 1/70, *ddr-2(qy64)* n = 4/60, *ina-1* RNAi n = 22/66, and *ddr-2(qy64)*; *ina-1* RNAi n = 31/60 animals with uterine prolapse respectively. ****$P \leq 0.0001$, *$P \leq 0.05$; Fisher's exact test. (**D**) Frequency of utse-seam detachments in late L4 wild-type and *ddr-2(qy64)* animals treated with control or *ina-1* RNAi. Control n = 0/21, *ina-1* RNAi n = 0/25, *ddr-2(qy64)* n = 2/21, and *ddr-2(qy64)*; *ina-1* RNAi n = 9/21 animals with detachments respectively. ***$P \leq 0.001$, *$P \leq 0.05$; Fisher's exact test. (**E**) Schematic of dominant negative (DN) β integrin *pat-3*. (**F**) Ventral fluorescence z-projections of the utse *(cdh-3p::mCherry::PLC$^{\delta PH}$* or *nas-22p::2xmKate2::PLC$^{\delta PH}$)* and seam *(wrt-2p::GFP::PLC$^{\delta PH}$* or *scmp::GFP::CAAX)* cells in late L4 wild-type animals and animals expressing *DN integrin* in the utse (*zmp-1$^{mk50-51}$* promoter) or the seam (*wrt-2* promoter). Dotted lines with asterisks indicate regions of utse-seam detachment. (**G**) Percentage of animals with utse-seam detachment. Wild type, n = 0/19; *DN integrin (utse)*, n = 4/18; *DN integrin (seam)*, n = 4/16 animals with detachments respectively. *$P \leq 0.05$, Fisher's exact test. Scale bars, 20 μm.

**Source data 1.** Source data for ***Figure 5***. Raw data of INA-1/PAT-2 fluorescence intensity quantification used to generate ***Figure 5B*** in Microsoft Excel format.
**Source data 2.** Source data for ***Figure 5—figure supplement 1***. Raw data of fluorescence intensity quantification of matrix components and ZMP-4 at the utse-seam BM-BM linkage used to generate boxplots in ***Figure 5—figure supplement 1*** in Microsoft Excel format.
**Source data 3.** Source data for ***Figure 5—figure supplement 2***. Raw data of fluorescence intensity quantification of *ina-1* knockdown used to generate plots in ***Figure 5—figure supplement 2D and E*** in Microsoft Excel format.

**Figure supplement 1.** *ddr-2* loss does not reduce functional levels of fibulin, hemicentin, type IV collagen, and matrix metalloproteinase ZMP-4 at the utse-seam connection; related to ***Figure 5***.
**Figure supplement 2.** The integrin α subunits INA-1 and PAT-2 are localized within both the utse and seam cells; related to ***Figure 5***.

## Figure 5—figure supplement 1

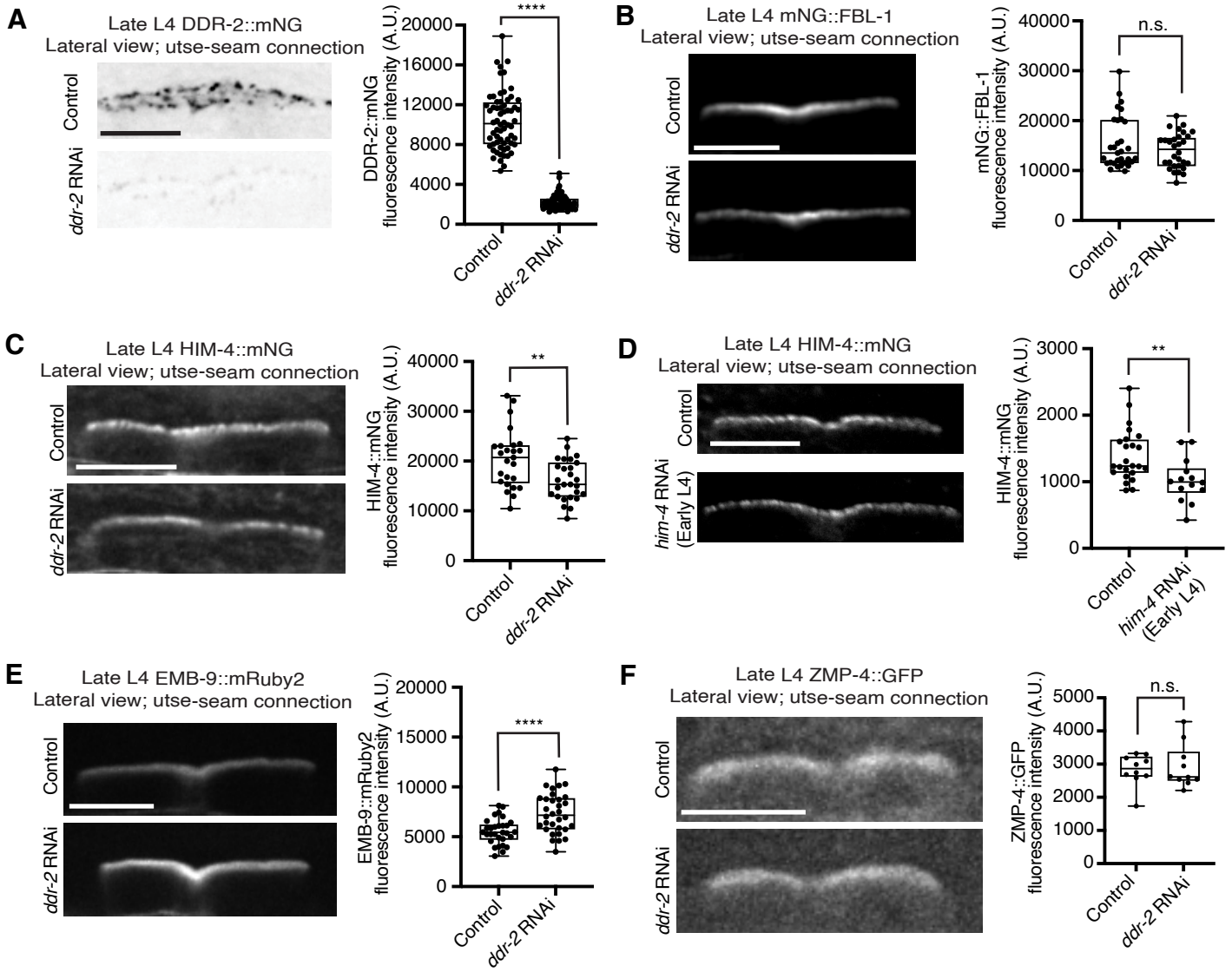


***ddr-2* loss does not reduce functional levels of fibulin, hemicentin, type IV collagen, and matrix metalloproteinase ZMP-4 at the utse-seam connection.** Related to ***Figure 5***. (**A**) Lateral fluorescence images of DDR-2::mNG at the utse-seam BM-BM connection in late L4 control or *ddr-2* RNAi-treated animals. Mean fluorescence intensity quantified on the right (n ≥ 60 all treatments). ****$P \leq 0.0001$, Mann-Whitney *U* test. (**B**) Lateral fluorescence images of mNG::FBL-1 (fibulin) at the utse-seam connection in late L4 control or *ddr-2* RNAi-treated animals. Mean fluorescence intensity quantified on the right (n ≥ 30 all treatments). n.s. (not significant), $P > 0.05$, Mann-Whitney *U* test. (**C**) Lateral fluorescence images of HIM-4::mNG (hemicentin) at the utse-seam tissue linkage in late L4 control or *ddr-2* RNAi-treated animals. Mean fluorescence intensity quantified on the right (n ≥ 25 all treatments). **$P \leq 0.01$, unpaired two-tailed Student's *t* test. (**D**) Lateral fluorescence images of HIM-4::mNG (hemicentin) at the utse-seam connection in late L4 control or *him-4* RNAi-treated animals. RNAi was initiated at the early L4 stage. Mean fluorescence intensity quantified on the right (n ≥ 14 all treatments). **$P \leq 0.01$, unpaired two-tailed Student's *t* test.
(**E**) Lateral fluorescence images of EMB-9::mRuby2 (type IV collagen) at the utse-seam attachment site in late L4 control or *ddr-2* RNAi-treated animals. Mean fluorescence intensity quantified on the right (n ≥ 30 all treatments). ****$P \leq 0.0001$, unpaired two-tailed Student's *t* test. (**F**) Lateral fluorescence images of matrix metalloproteinase ZMP-4::GFP at the utse-seam tissue connection in late L4 control or *ddr-2* RNAi-treated animals. Mean fluorescence intensity quantified on the right (n = 10 all treatments). n.s. (not significant), $P > 0.05$, Mann-Whitney *U* test. Scale bars, 20 $\mu$m. Box edges in boxplots represent the 25th and 75th percentiles, the line in the box denotes the median value, and whiskers mark the minimum and maximum values.

## Figure 5—figure supplement 2

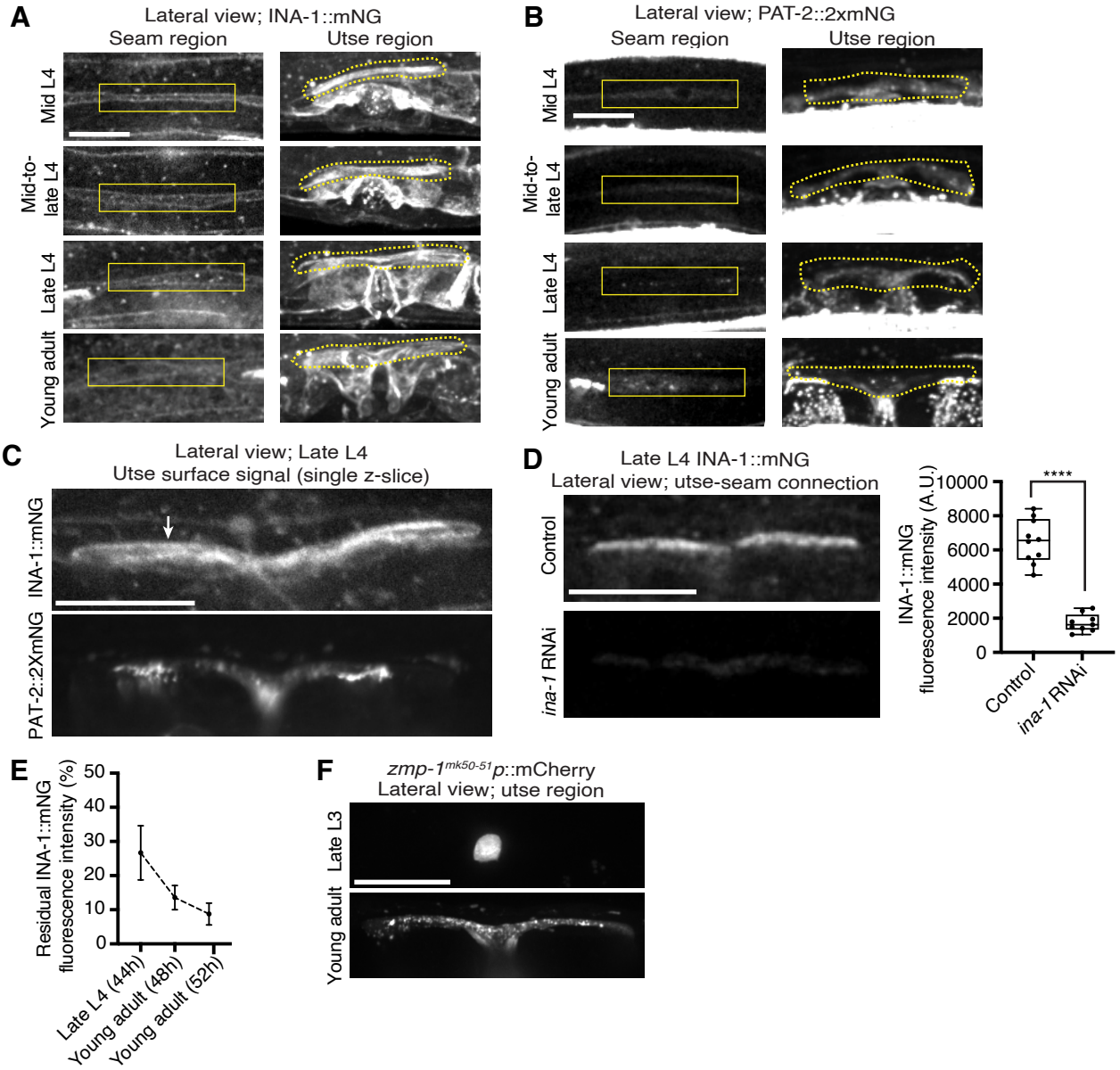


**The integrin α subunits INA-1 and PAT-2 are localized within both the utse and seam cells.**
Related to ***Figure 5***. (**A**) Lateral fluorescence z-projections of the integrin α subunit INA-1::mNG between the mid L4 and young adult stages. Localization in the seam and utse are indicated by solid and dotted boxed regions respectively (n ≥ 10 animals examined all stages). (**B**) Lateral fluorescence z-projections of the integrin α subunit PAT-2::2XmNG between the mid L4 and young adult stages. Localization in the seam and utse are indicated by solid and dotted boxed regions respectively (n ≥ 7 animals examined all stages). (**C**) Lateral fluorescence images of INA-1::mNG and PAT-2::2XmNG at the z-plane of the utse surface in late L4 animals (n ≥ 10 animals examined each). Arrow indicates strong INA-1 signal at the utse surface. (**D**) Lateral fluorescence images of INA-1::mNG at the utse-seam connection in late L4 control or *ina-1* RNAi-treated animals. Mean fluorescence intensity quantified on the right (n ≥ 9 all treatments). ****$P \leq 0.0001$, unpaired two-tailed Student's *t* test. (**E**) Quantification of residual INA-1::mNG fluorescence intensity at the utse-seam interface at the indicated developmental stages following *ina-1* knockdown initiated at the L1 stage. Data are represented as percentages of mean INA-1::mNG at the respective stages in control animals (n ≥ 7 animals examined all stages). Error bars denote SD. (**F**) Lateral fluorescence z-projections of mCherry driven by the *zmp-1*$^{mK50-51}$ promoter in the utse region in late L3 and young adult animals (n = 5 animals examined at each stage).

## **Figure 6** with 1 supplement

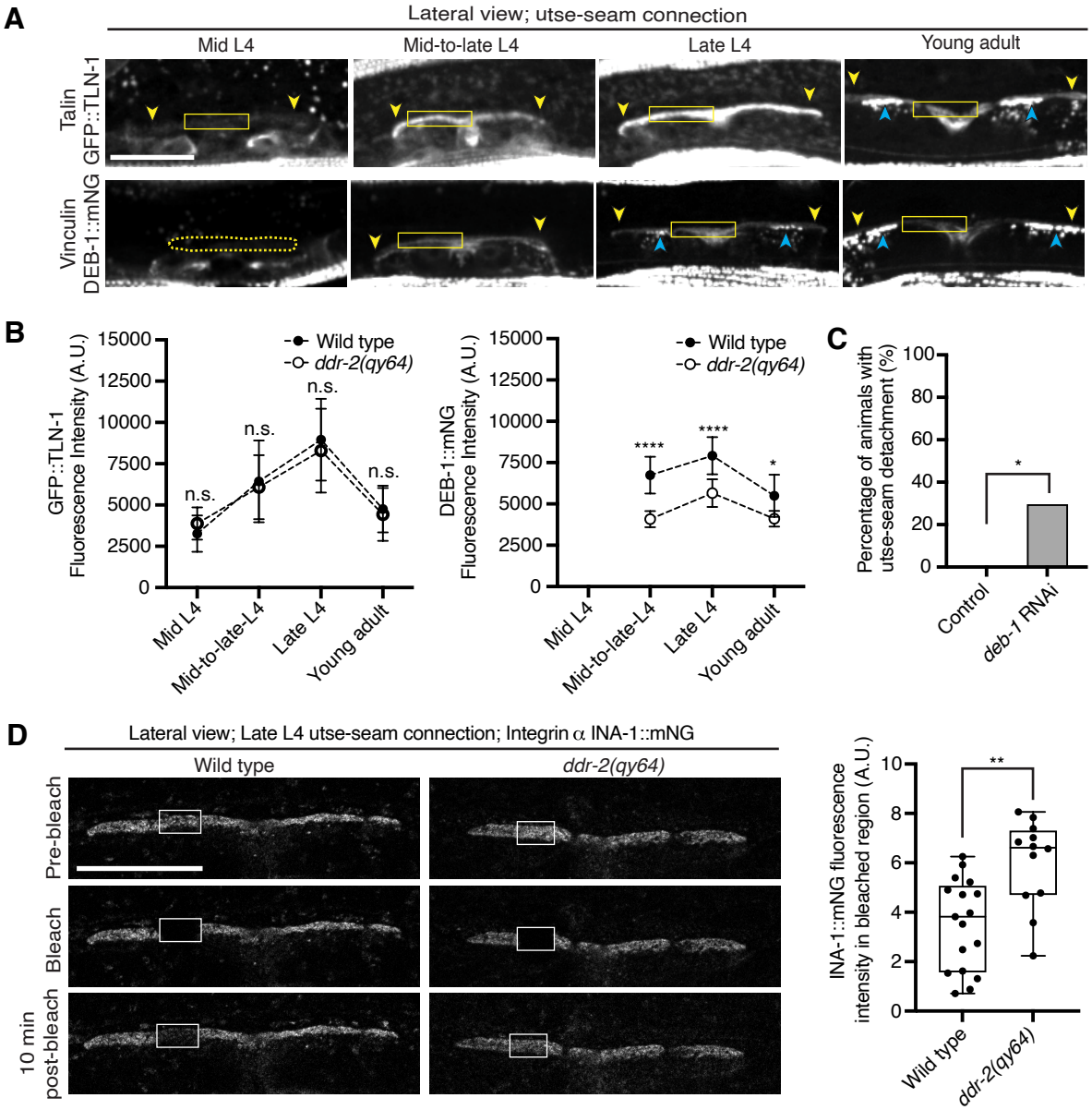


**DDR-2 upregulates vinculin levels and stabilizes integrin at the utse-seam connection.**
(**A**) Lateral fluorescence z-projections of the integrin activators talin (GFP::TLN-1) and vinculin (DEB-1::mNG) at the utse-seam attachment region (bounded by yellow arrowheads) from the mid L4 to young adult stages. Vinculin was not detected at the utse-seam attachment region at the mid L4 stage (dotted yellow box). Blue arrowheads indicate fluorescence signal at muscle attachment sites. Fluorescence intensity at the utse-seam attachment region was measured in the solid yellow boxes. (**B**) Quantification of TLN-1 and DEB-1 mean fluorescence intensity in wild-type and *ddr-2* knockout *(ddr-2(qy64))* animals (n ≥ 9 all conditions). Error bars represent SD. ****$P \leq 0.0001$, **$P \leq 0.01$, *$P \leq 0.05$, n.s. (not significant), $P > 0.05$; unpaired two-tailed Student's *t* test. (**C**) Frequency of utse-seam detachments observed in control or *deb-1* RNAi-treated late L4 animals. Control n = 0/21, *ina-1* RNAi n = 5/17 animals with detachments respectively. *$P \leq 0.05$, Fisher's exact test. (**D**) Left: Lateral fluorescence images of INA-1::mNG at the utse-seam connection before photobleaching, immediately after photobleaching, and 10 min post-photobleaching in late L4 wild-type and *ddr-2(qy64)* animals. Box indicates bleached region. Right: Quantification of mean INA-1::mNG fluorescence intensity in the bleached region 10 min post-photobleaching. Wild type, n = 17; *ddr-2(qy64)*, n = 12. **$P \leq 0.01$, unpaired two-tailed Student's *t* test. Scale bars, 20 μm. Box edges in boxplots represent the 25th and 75th percentiles, the line in the box denotes the median value, and whiskers mark the minimum and maximum values.

**Source data 1.** Source data for ***Figure 6***. Raw data of fluorescence intensity quantification of TLN-1 and DEB-1 as well as INA-1 recovery after photobleaching used to generate plots in ***Figure 6B and D*** in Microsoft Excel format.
**Source data 2.** Source data for ***Figure 6—figure supplement 1***. Raw data of fluorescence intensity quantification of *deb-1* knockdown at the utse-seam connection used to generate boxplot in ***Figure 6—figure supplement 1*** in Microsoft Excel format.

**Figure supplement 1.** *deb-1* knockdown efficiency; related to ***Figure 6C***.

## Figure 6—figure supplement 1

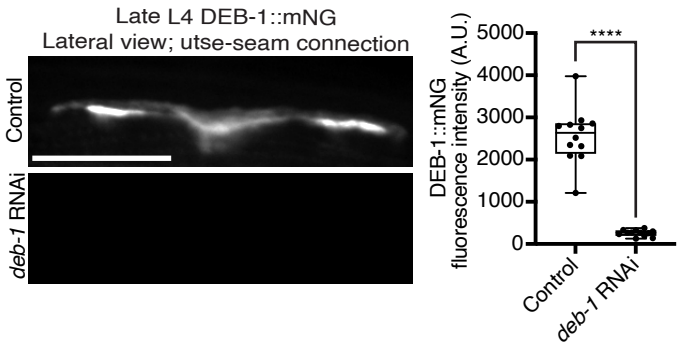


***deb-1* knockdown efficiency.**
Related to ***Figure 6***. Lateral fluorescence images of DEB-1::mNG (vinculin) at the utse-seam connection in late L4 control or *deb-1* RNAi-treated animals. Mean fluorescence intensity quantified on the right (n = 12 all treatments). ****$P \leq 0.0001$, unpaired two-tailed Student's *t* test. Scale bars, 20 $\mu$m. Box edges in boxplots represent the 25th and 75th percentiles, the line in the box denotes the median value, and whiskers mark the minimum and maximum values.

## **Figure 7** with 1 supplement

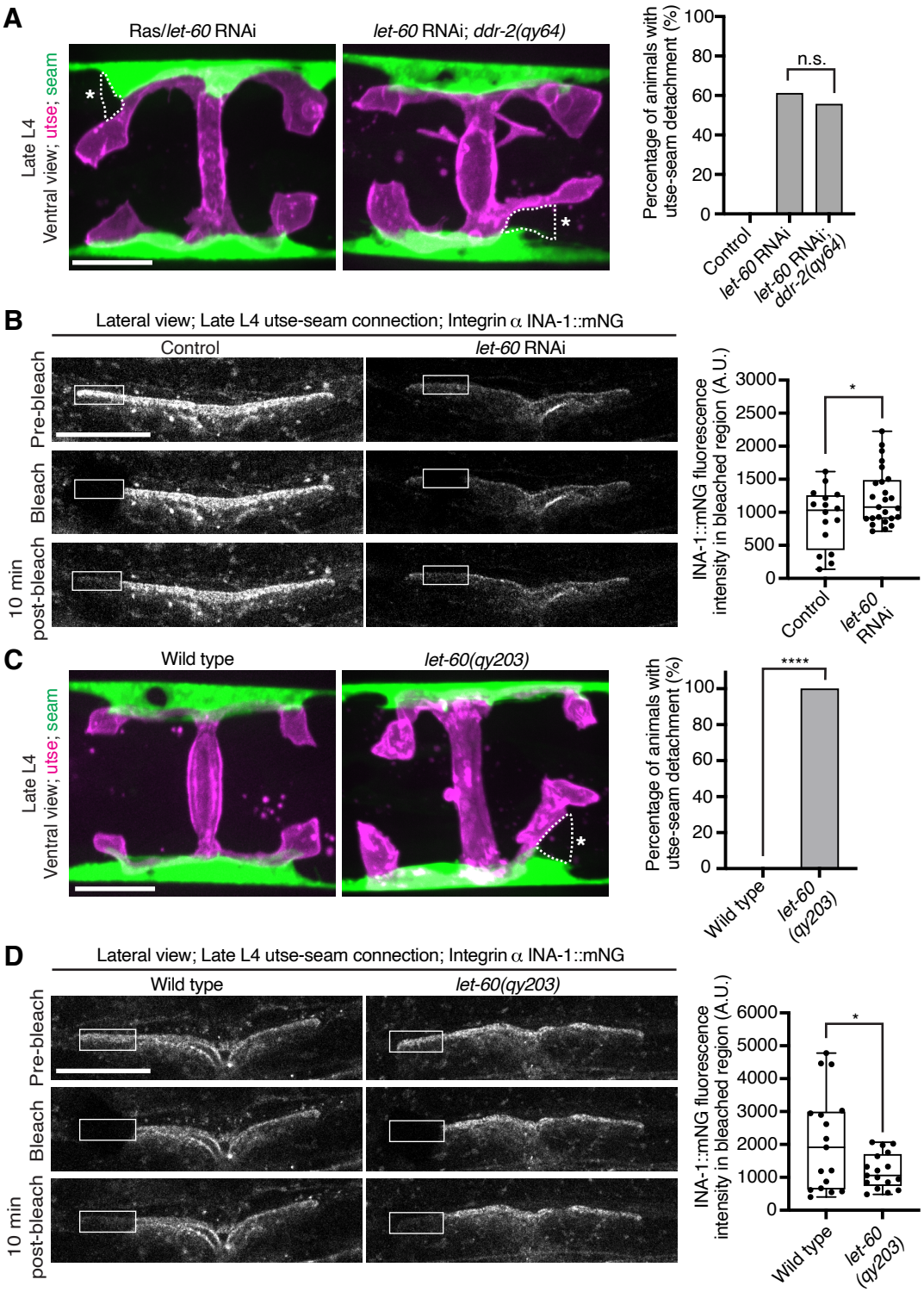


**Ras/LET-60 acts in the same pathway as DDR-2 and controls integrin stability at the utse-seam tissue connection.**
(**A**) Left: Ventral fluorescence z-projections of the utse *(nas-22p::2xmKate2::PLC $^{\delta PH}$)* and seam *(scmp::GFP::CAAX)* tissues in wild-type and *ddr-2* knockout *(ddr-2(qy64))* animals on Ras/*let-60* RNAi treatment. Dotted lines with asterisks indicate regions of utse-seam detachment. Right: Percentage of animals with utse-seam detachment. Control n = 0/21, *let-60* RNAi n = 11/18, and *let-60* RNAi; *ddr-2(qy64)*, n = 10/18 animals with detachments respectively. n.s. (not significant), $P > 0.05$; Fisher's exact test. (B) Left: Lateral fluorescence images of INA-1::mNG at the utse-seam connection before photobleaching, immediately after photobleaching, and 10 min post-photobleaching in late L4 control or *let-60* RNAi-treated animals. Box indicates bleached region. Right: Quantification of mean INA-1::mNG fluorescence intensity in the bleached region 10 min post-photobleaching. Control n = 16, *let-60* RNAi n = 25. *$P \leq 0.05$, unpaired two-tailed Student's *t* test. (C) Left: Ventral fluorescence z-projections of the utse and seam tissues in late L4 wild-type and *let-60* gain-of-function mutant *(let-60(qy203))* animals. Dotted lines with asterisks indicate regions of utse-seam detachment. Right: Quantification of utse-seam detachment frequency. Wild type, n = 0/26; *let-60(qy203)*, n = 11/11 animals with detachments respectively. ****$P \leq 0.0001$, Fisher's exact test. (D) Left: Lateral fluorescence images of INA-1::mNG at the utse-seam attachment region before photobleaching, immediately after photobleaching, and 10 min post-photobleaching in late L4 wild-type and *let-60(qy203)* animals. Box indicates bleached region. Right: Quantification of mean INA-1::mNG fluorescence intensity in the bleached region 10 min post-photobleaching (n = 17 each genotype). *$P \leq 0.05$, unpaired two-tailed Student's *t* test. Scale bars, 20 μm. Box edges in boxplots represent the 25th and 75th percentiles, the line in the box denotes the median value, and whiskers mark the minimum and maximum values.

**Source data 1.** Source data for ***Figure 7***. Raw data of fluorescence intensity quantification of INA-1::mNG for photobleaching experiments used to generate boxplots in ***Figure 7B and D*** in Microsoft Excel format. Note that source data for ***Figure 7—figure supplement 1*** is found within ***Source data 1***.

**Figure supplement 1.** Ras/*let-60* knockdown reduces INA-1::mNG levels at the utse-seam connection; related to ***Figure 7B***.

# Figure 7—figure supplement 1

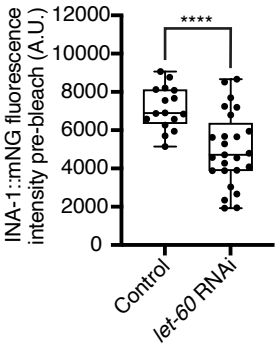


**Ras/*let-60* knockdown reduces INA-1::mNG levels at the utse-seam connection.**
Related to ***Figure 7***. Quantification of mean INA-1::mNG fluorescence intensity at the utse-seam connection prior to photobleaching in control or Ras/*let-60* RNAi-treated late L4 animals (see representative images in ***Figure 7B***, pre-bleach panel. Control n = 16; *let-60* RNAi n = 25. ****$P \leq 0.0001$, unpaired two-tailed Student's *t* test. Scale bars, 20 $\mu$m. Box edges in boxplots represent the 25th and 75th percentiles, the line in the box denotes the median value, and whiskers mark the minimum and maximum values.

## Figure 8

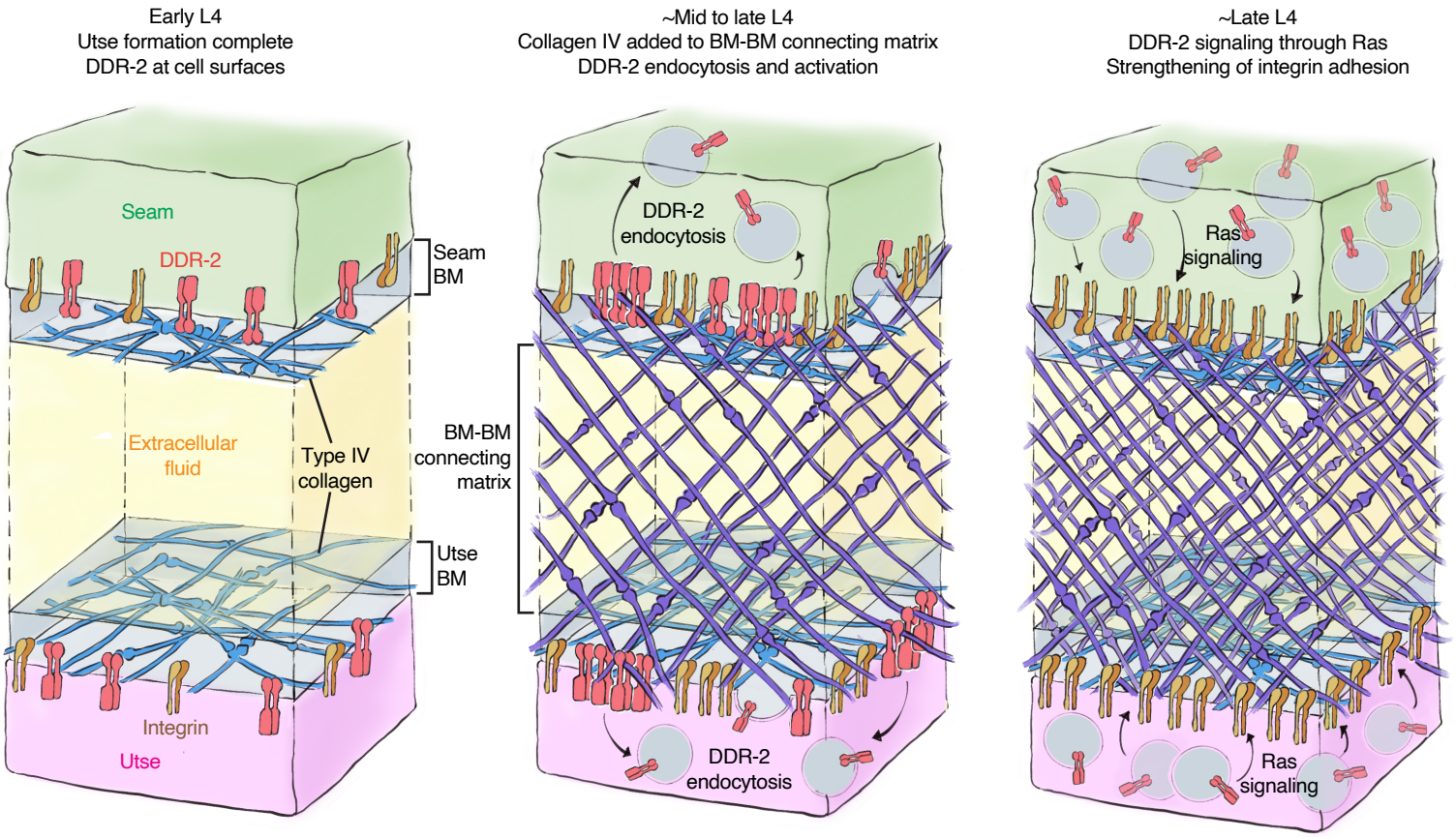


**Model of DDR-2 function at the utse-seam tissue connection.**
(**A**) At the early L4 larval stage, DDR-2 is predominantly found at the surfaces of utse and seam cells. (**B**) Between the mid and late L4 stages, type IV collagen assembles in the BM-BM connecting matrix to link the utse and seam tissues. Collagen addition and binding to DDR-2 triggers DDR-2 endocytosis and activation. (**C**) By the late L4, endocytic localization of DDR-2 reaches peak levels. Ras/LET-60 acts in the same pathway and may function downstream of DDR-2 to stabilize integrin adhesion. Thus, type IV collagen has a dual role in fastening the tissue connection and in signaling through DDR-2 to bolster cell adhesion at the linkage site.